AGSC

PRELIMINARY RESULTS OF PIMA ANALYSES OF THE ALTERATION ZONE UNDERLYING THE SULPHUR SPRINGS DEPOSIT, PANORAMA DISTRICT, PILBARA BLOCK, WESTERN AUSTRALIA

by

David L. Huston, Julienne Kamprad and Carl Brauhart

AGSO RECORD 1997/14

AGSO

AUSTRALIAN GEOLOGICAL SURVEY ORGANISATION

PRELIMINARY RESULTS OF PIMA ANALYSES OF THE ALTERATION ZONE UNDERLYING THE SULPHUR SPRINGS DEPOSIT, PANORAMA DISTRICT, PILBARA BLOCK, WESTERN AUSTRALIA

by

David L. Huston, Julienne Kamprad and Carl Brauhart

AGSO RECORD 1997/14

PRELIMINARY RESULTS OF PIMA ANALYSES OF THE ALTERATION ZONE UNDERLYING THE SULPHUR SPRINGS DEPOSIT, PANORAMA DISTRICT, PILBARA BLOCK, WESTERN AUSTRALIA

BY

DAVID L. HUSTON[1], JULIENNE KAMPRAD[1] AND CARL BRAUHART[2]

[1]Australian Geological Survey Organisation, G.P.O. Box 378, Canberra, ACT 2601
[2]Key Centre for Strategic Minerals, University of Western Australia, Nedlands, WA 6907

AGSO RECORD 1997/14

DEPARTMENT OF PRIMARY INDUSTRIES AND ENERGY

Minister for Primary Industries and Energy: Hon. J. Anderson, M.P.
Minister for Resources and Energy: Senator the Hon. W.R. Parer
Secretary: Paul Barratt

AUSTRALIAN GEOLOGICAL SURVEY ORGANISATION

Executive Director: Neil Williams

ISSN: 1039-0073
ISBN: 0 642 25020 0

Abstract

To assess the efficacy of the PIMA (Portable Infrared Mineral Analyser) as an exploration tool for VHMS (volcanic-hosted massive sulphide) exploration, a trial study was undertaken in rocks underlying the Sulphur Springs deposit in the central Pilbara, Western Australia. PIMA spectra indicate the presence of chlorite, sericite and kaolinite as alteration minerals in this region. The wavelength and depth of Al-OH and Fe-OH absorption peaks were measured. The spatial distribution of the depth ratio of Fe-OH to Al-OH absorption peaks maps out known zones of chlorite-quartz alteration efficiently and has high potential as an exploration guide. This ratio is related to the chlorite-sericite ratio. The wavelength of the Fe-OH peak, which relates to chlorite composition, was also found to have potential as an exploration guide.

Introduction

To complement ongoing geological, geochemical and isotopic studies of semi-regional alteration zones associated volcanic-hosted massive sulphide (VHMS) deposit, a PIMA (Portable Infrared Mineral Analyser) study has been undertaken on with the Sulphur Springs deposit to evaluate its potential use in mineral exploration and ore genesis studies. This document presents preliminary results of this study.

How does the PIMA work?

The PIMA is a spectrometer that measures the infrared reflectance over the short wavelength infrared (SWIR) between 1300 and 2500 nm from a sample that has been illuminated with light having wavelengths between 1300 and 2500 nm. The spectral responses of geological samples (rocks or rock powders) is caused by the absorbance of light at characteristic wavelengths owing to the vibration of inter-molecular bonds. Although the molecular absorptions occur in the mid-infrared part of the spectrum, the PIMA measures the harmonics of the "fundamental" absorptions in the SWIR part of the spectrum.

The absorptions observed in SWIR are mostly related to bonds in hydroxyl (OH^-), water (H_2O), carbonate (CO_3^{2-}) and ammonium (NH_4^+) groups in minerals. Hydroxyl vibrations combine with lattice vibrations to produce vibrations between hydroxyl and Al, Fe and Mg atoms. Hence, common alteration minerals such as phyllosilicates and carbonates lend themselves to PIMA analysis (Pontual and Merry, 1995).

Geology

The geological setting of the Sulphur Springs VHMS deposit, which has been described by Morant (1995), Brauhart (1996, 1997), and Brauhart and Morant (1997), is shown in Figure 1. The deposit, which contains a geological resource of 6.2 Mt at 6% Zn and 2% Cu, is associated with chert that marks the contact between underlying volcanic rocks of the Strelley Sequence and overlying Gorge Creek Group greywacke and shale (Morant, 1995). The basal unit of the Strelley Sequence consistes of massive to pillowed andesitic lava; Brauhart (1996) has split this unit into two subunits: underlying "felsic" andesite and overlying "true" andesite. The andesitic rocks are overlain by dacite, which McPhie and Goto (in Morant, 1995) interpret as shallow sills. Several lenses of rhyodacite occur in the marker chert west of the deposit.

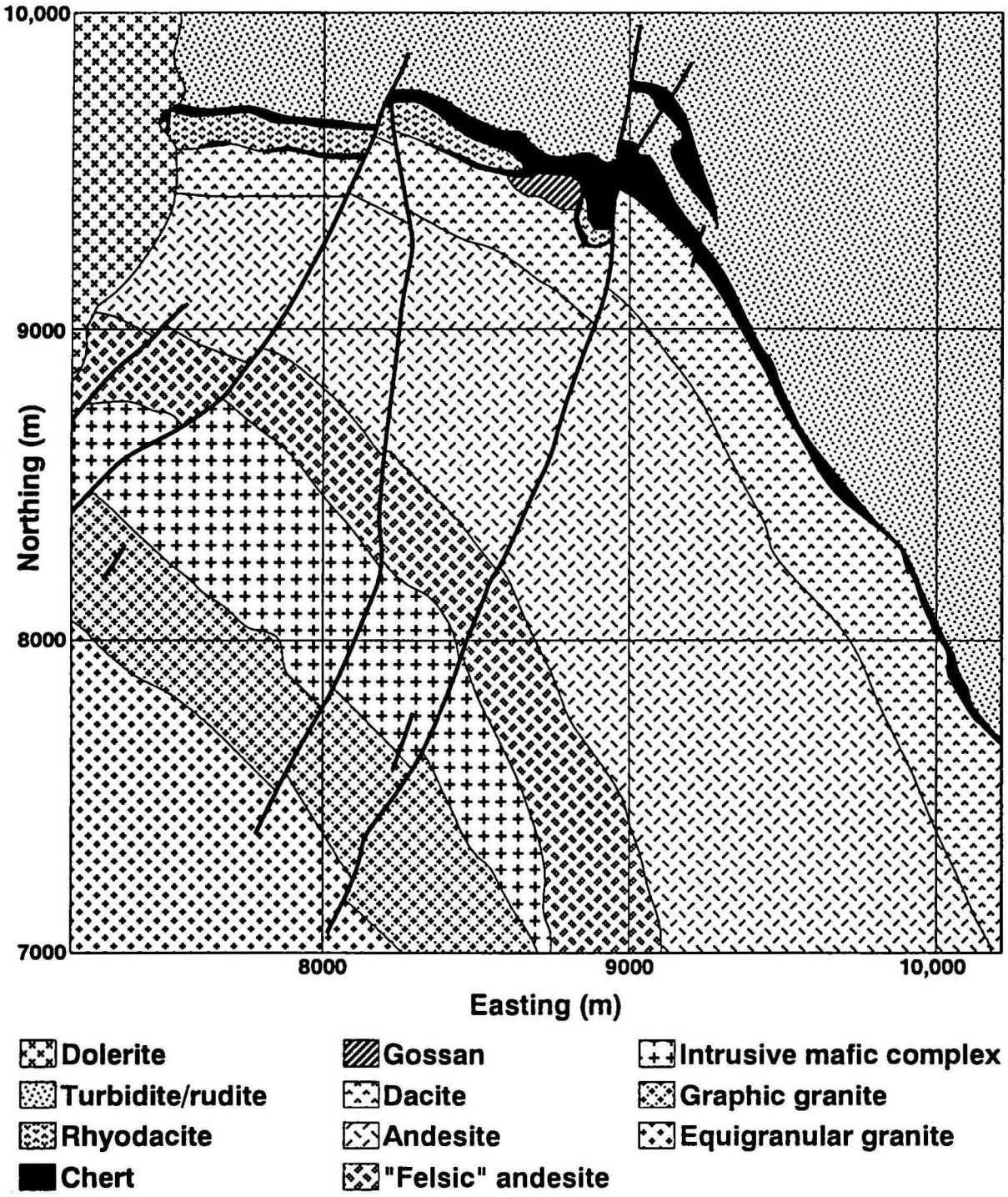

Figure 1. Geology of the Sulphur Springs area (data of C. Brauhart and P. Morant).

Mapping of the subvolcanic Strelley Granite by Brauhart (1997) indicates the presence of two major phases: (1) an equigranular outer phase, and (2) a quartz-feldspar-phyric inner phase (not shown in Fig. 1). The marginal part of the equigranular granite has a granophyric texture. The contact between the granophyric granite and the volcanic sequence is intruded by a later mafic intrusive complex (Brauhart, 1997). A dolerite dike occupies a fault that offsets the Strelley Sequence west of the Sulphur Springs deposit.

Brauhart and Morant (1997) have mapped alteration zonation in the Strelley Sequence, including that underlying Sulphur Springs deposit (Fig. 2). They recognised three main alteration assemblages: (1) chlorite-quartz-albite±carbonate±pyrite, which is the regional "background" alteration assemblage, (2) chlorite-quartz, which forms a pipe-like zone underneath Sulphur Springs and a semi-conformable zone at the base of the andesite, and (3) sericite-dominant, which occurs mainly in dacite lateral to the Sulphur Springs deposit.

Methodology

To allow direct comparison with ongoing alteration studies, PIMA analyses were undertaken on 63 rock powders that are also being analysed for whole rock geochemistry and oxygen isotopes. For this preliminary study, the PIMA results are compared with existing mineralogical data and the oxygen isotope data.

Raw spectra measured by PIMA are influenced by absorptions outside of the spectral range of the PIMA (e.g. ferrous iron at 1000 nm and water and carbonate at 2700 nm; Pontual and Merry, 1995). Consequently, the raw (or reflectance) spectra are difficult to interpret. To overcome this problem, the gross curvature of the spectra (i.e. the hull) was removed by dividing the reflectance spectra into the fitted hull. The spectra shown in Figures 3 and 4 are the end result of this transformation.

The resulting spectra were then classified by shape into spectral groups prior to further processing. Several examples of each spectral group were then inspected in detail to determine the probable hydrous and carbonate minerals present. In most cases, minerals other than these two groups cannot be identified using PIMA analysis. Although not quantified, some minerals may not be detectable unless they are present in high abundances.

The following parameters were then measured, when present, from each spectrum: the depth and position of the peak within the Al-OH (2180-2220 nm) and Fe-OH (2230-2295 nm) absorbance bands. These parameters and ratios between these parameters were compared with the distribution of alteration assemblages and oxygen isotope data. Future work will be aimed at acquiring and interpreting data from other absorbance bands.

Results

Table 1 summarises the characteristics of spectral groups into which the PIMA spectra were classified. Figures 3 and 4 illustrate sample spectra from all spectral groups. Two spectra (207177 and 207502) did not fit into any spectral group. Comparison of the spectral groups with alteration assemblages determined in the field indicate that some spectral groups correspond to alteration assemblages (Table 1). For instance, all group A1 spectra came from sericite-quartz altered rocks; all group B1 spectra came from chlorite-quartz altered rocks; and all group B2 and B3 spectra came from "background" altered rocks. A pyroxenite sample (207502) from the mafic intrusive complex had a unique PIMA spectra.

Mineral species identified using PIMA

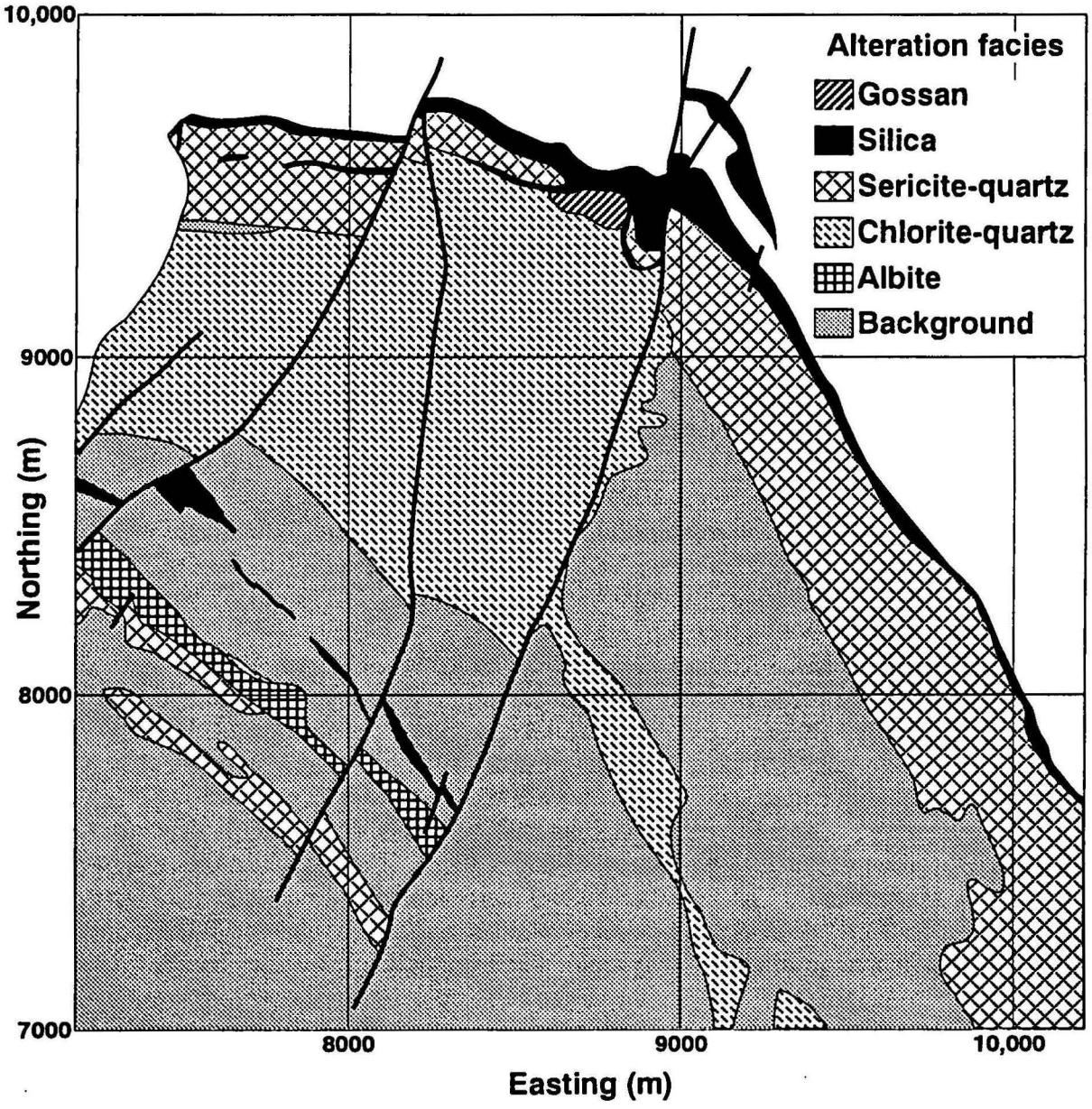

Figure 2. Alteration map of the Sulphur Springs area (data of C. Brauhart).

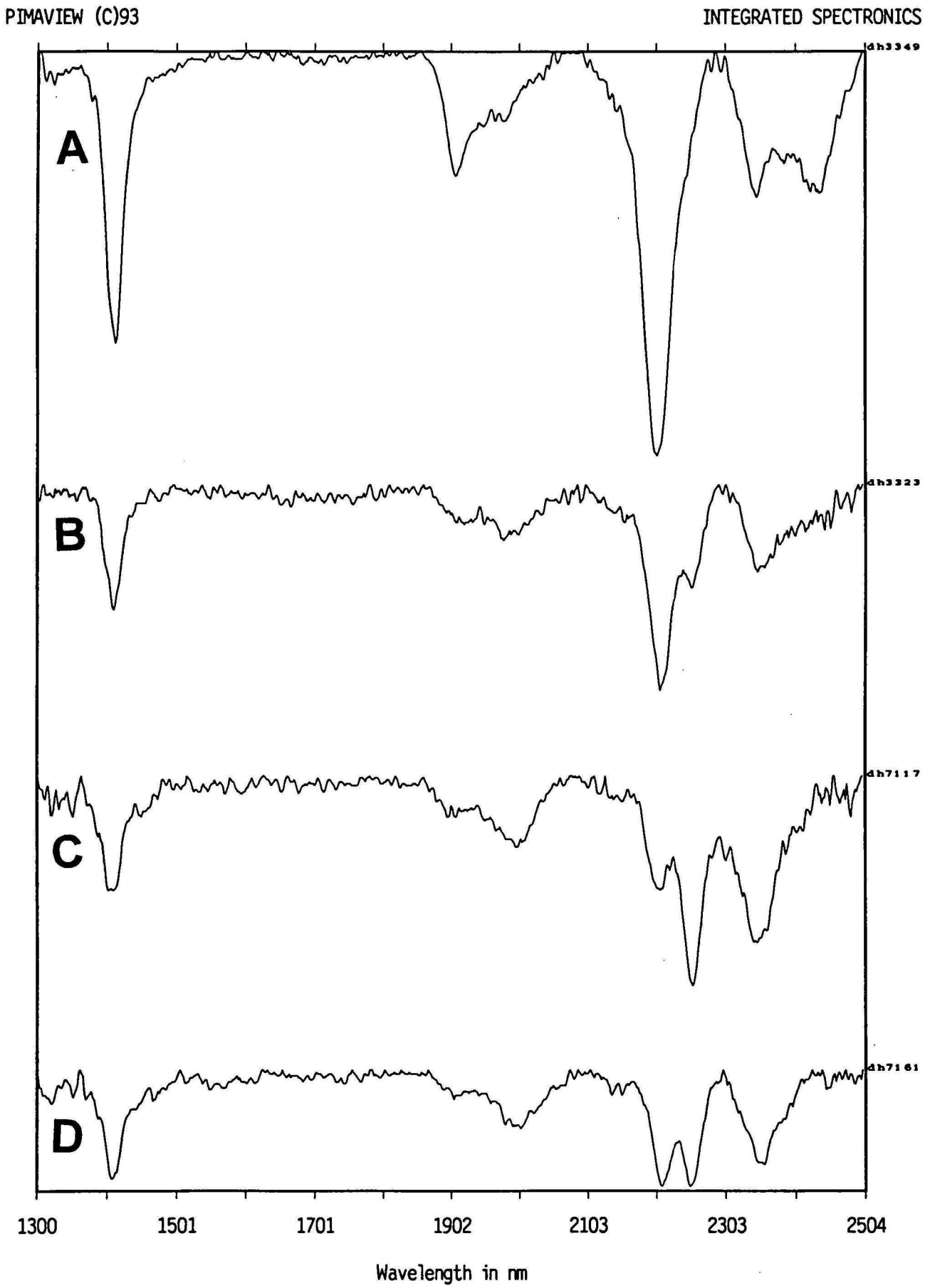

Figure 3. Sample hull quotient PIMA spectra for samples (a) 203349 (Group A1), (b) 203323 (Group A2), (c) 207117 (Group B1), and (d) 207161 (Group B2)

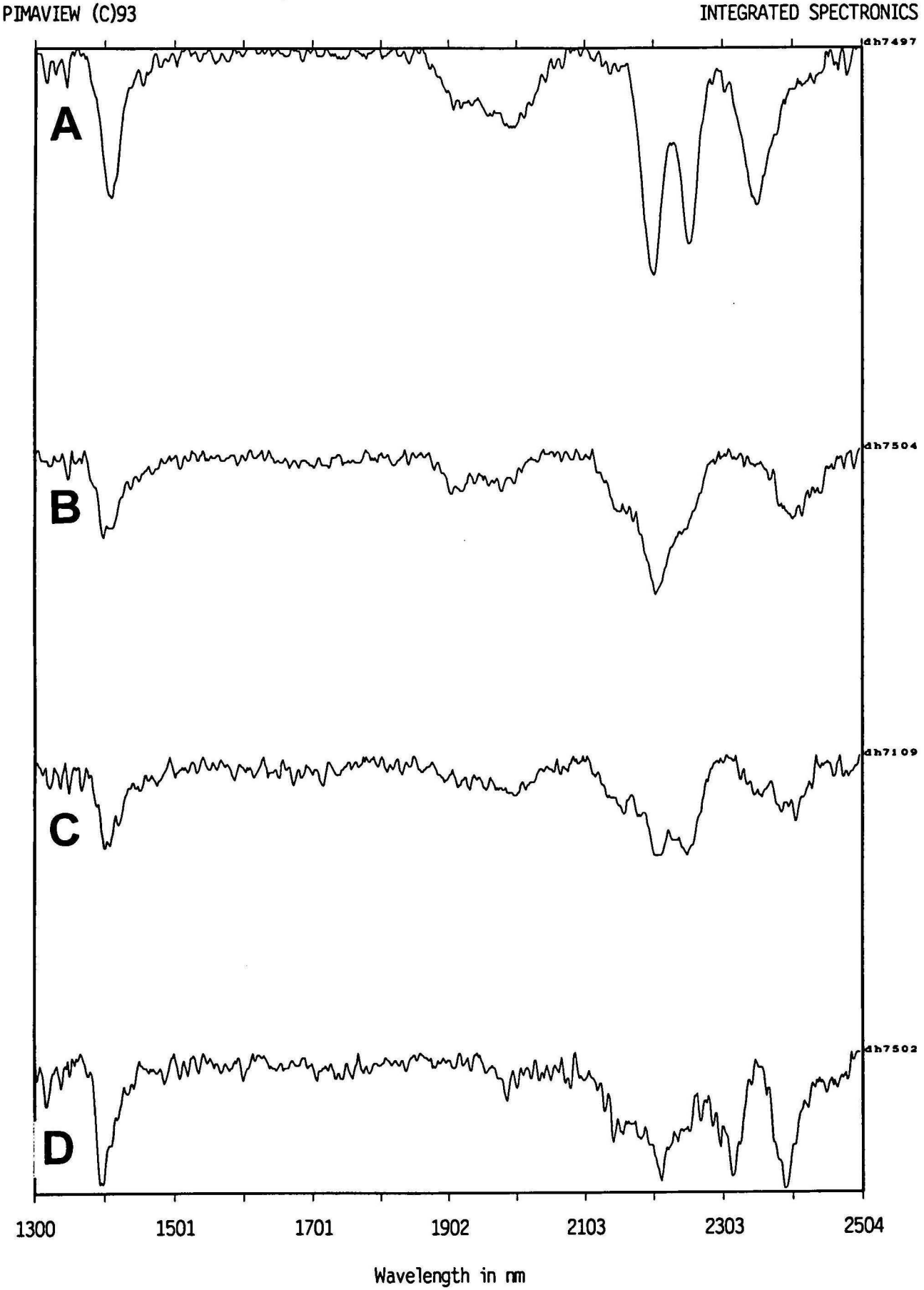

Figure 4. Sample hull quotient PIMA spectra for samples (a) 207497 (Group B3), (b) 207504 (Group C), (c) 207109 (Group D), and (d) 207502 (Other).

Table 1. Characteristics of PIMA spectral groups, based on samples from semi-regional alteration zones associated with the Sulphur Springs volcanic-hosted massive sulphide deposit.

Spectral group	Spectral characteristics	Corresponding alteration assemblages	Inferred mineral assemblage from PIMA spectra
A1	Al-OH and OH spectral peaks only; good quality spectra.	Sericite	Sericite
A2	Al-OH spectral peaks >> Fe-OH spectral peaks; good quality spectra.		Sericite >> chlorite
B1	Fe-OH spectral peaks >> Al-OH spectral peaks; good quality spectra.	Chlorite-quartz	Chlorite >> sericite
B2	FeOH spectral peaks ~ Al-OH spectral peaks; poor to moderate quality spectra.	"Background"	Chlorite ~ sericite ± kaolinite (?)
B3	FeOH spectral peaks ~ Al-OH spectral peaks; good quality spectra.	"Background"	Chlorite ~ sericite
C	Al-OH and OH spectral peaks only; poor to moderate quality spectra.		Sericite
D	FeOH spectral peaks ~ Al-OH spectral peaks; poor to moderate quality spectra.		Chlorite ± sericite ± kaolinite (?)

With the exception of sample 207502, the distinguishing features of spectral groups are the signal-to-noise ratio of the spectra, and the relative depths of the Al-OH and Fe-OH absorption peaks (Table 1). Qualitative examination of the spectra indicate that most spectra are dominated by chlorite and/or sericite: spectra from thirty-eight samples indicate the presence of both chlorite and sericite; twenty-four spectra indicate the presence of sericite, but not chlorite; and one spectrum indicate the presence of chlorite, but not sericite. The PIMA spectrum of sample 207502 indicates the presence of actinolite-tremolite and sericite (Fig. 4d). Several spectra showed small peaks at ~2160 nm (e.g. Fig. 4c), which is interpreted as indicating minor kaolinite.

The PIMA spectra do not indicate the presence of carbonate minerals, even though one of the characteristics of spilitically altered andesite is the presence of calcite. This apparent inconsistency results from the high abundance of carbonate minerals required before PIMA spectra indicate their presence. The PIMA spectra do not indicate the presence of other hydrous minerals in the samples analysed.

Measured spectral responses: spatial variations

Figure 5 shows the location of samples analysed in the study, and Figures 6 to 8 show spatial variations in responses for various parameters measured from the PIMA spectra. All data are summarised in Table 2.

Depth ratio of Fe-OH and Al-OH absorption peaks. Figure 6 shows the spatial variation of a ratio of the depth of peaks within the Fe-OH and Al-OH absorbance bands (e.g. $D_{[2240\text{-}2260]}/D_{[2200\text{-}2220]}$). Although complicated by other factors (see below), this ratio grossly corresponds to a chlorite/sericite ratio.

Inspection of Figure 6 indicates that higher $D_{[2240\text{-}2260]}/D_{[2200\text{-}2220]}$ values (> 0.5) correspond broadly to the chlorite-quartz zone as mapped by C. Brauhart. The highest values (> 2.0) occur in the andesite directly below the Sulphur Springs gossan and extend west to the major dolerite dike. A smaller, strataform, zone of high values (> 2.0) corresponds to the southeastern extension of the chlorite-quartz alteration zone at the base of the andesite.

PIMA analysis also indicates the presence of a 300-400 m wide, strataform zone with higher $D_{[2240\text{-}2260]}/D_{[2200\text{-}2220]}$ values (0.5-2.0) in the upper part of the background alteration zone southeast of the chlorite-quartz pipe. No corresponding change in mapped alteration mineralogy has been observed in this region.

Low $D_{[2240\text{-}2260]}/D_{[2200\text{-}2220]}$ values (< 0.5; generally 0.0) are restricted to sericite-dominant alteration zones, to the granite and mafic intrusive complex, and to the lower part of "background" altered andesite. In most cases, changes in $D_{[2240\text{-}2260]}/D_{[2200\text{-}2220]}$ are sharp; however, changes in this ratio between sericite-altered dacite and the upper part of "background" altered andesite are gradational.

Wavelength variations of the Fe-OH absorption band. Variations in the wavelength of the Fe-OH and the Mg-OH absorption bands can be used as a qualitative indication of chlorite composition. In this study, the Fe-OH absorption band (2240-2260 nm) was used, as in many samples, the Mg-OH absorption band was poorly defined. Low wavelength values indicate Mg-rich chlorite, whereas higher values indicate Fe-rich chlorite (Pontual and Merry, 1995).

Inspection of Figure 7 indicates that most Fe-OH absorbance peaks around Sulphur Springs are between 2255 and 2257 nm, which indicates Fe-rich chlorite. Values below 2255 nm are restricted to the northwestern part and the southeasternmost extension of the chlorite-quartz alteration zone. Values greater than 2257 nm are restricted to a small part of "background"-altered andesite with high $D_{[2240\text{-}2260]}/D_{[2200\text{-}2220]}$.

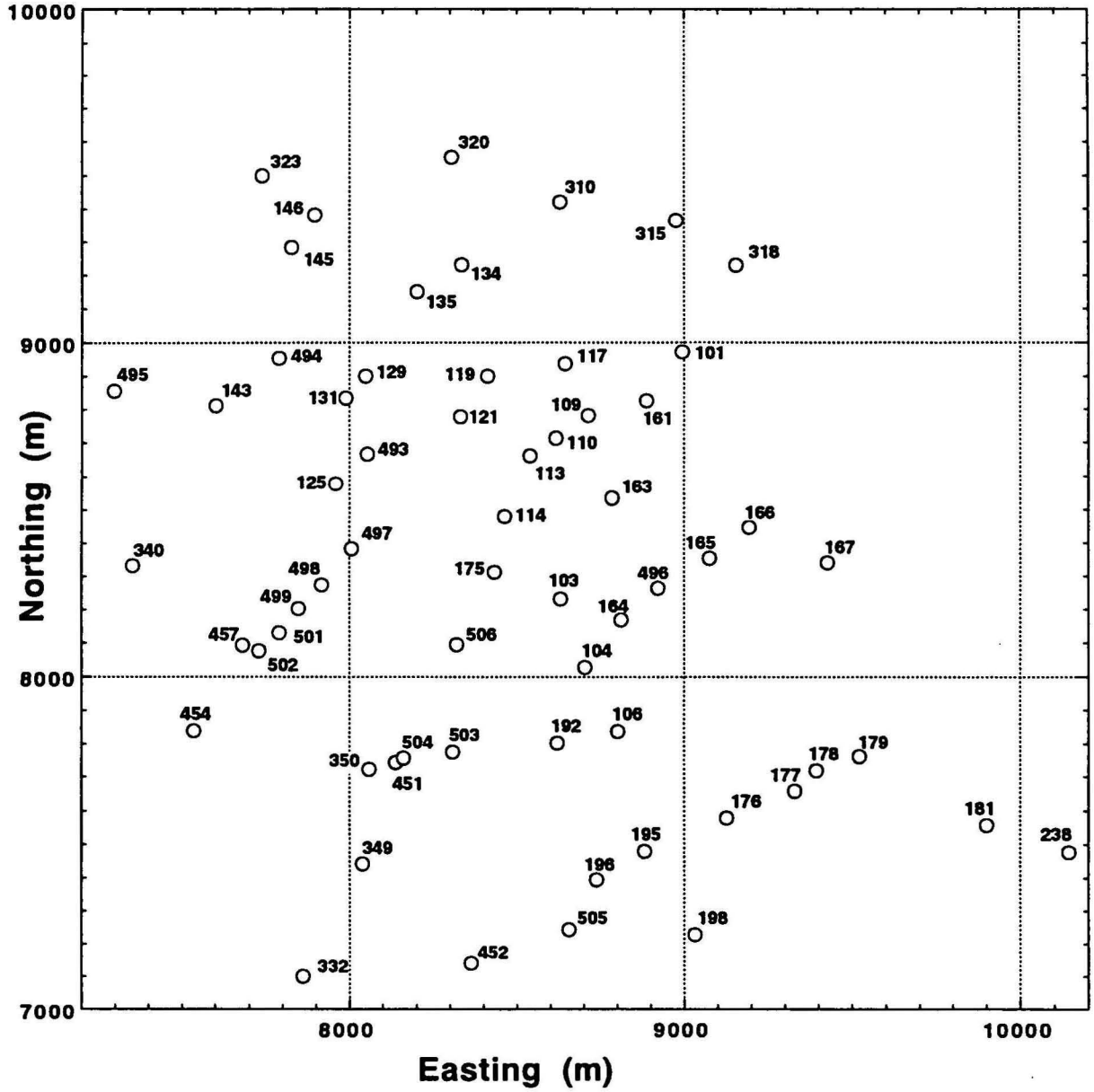

Figure 5. Location of samples analysed during this study (the last three digets of each sample number are indicated).

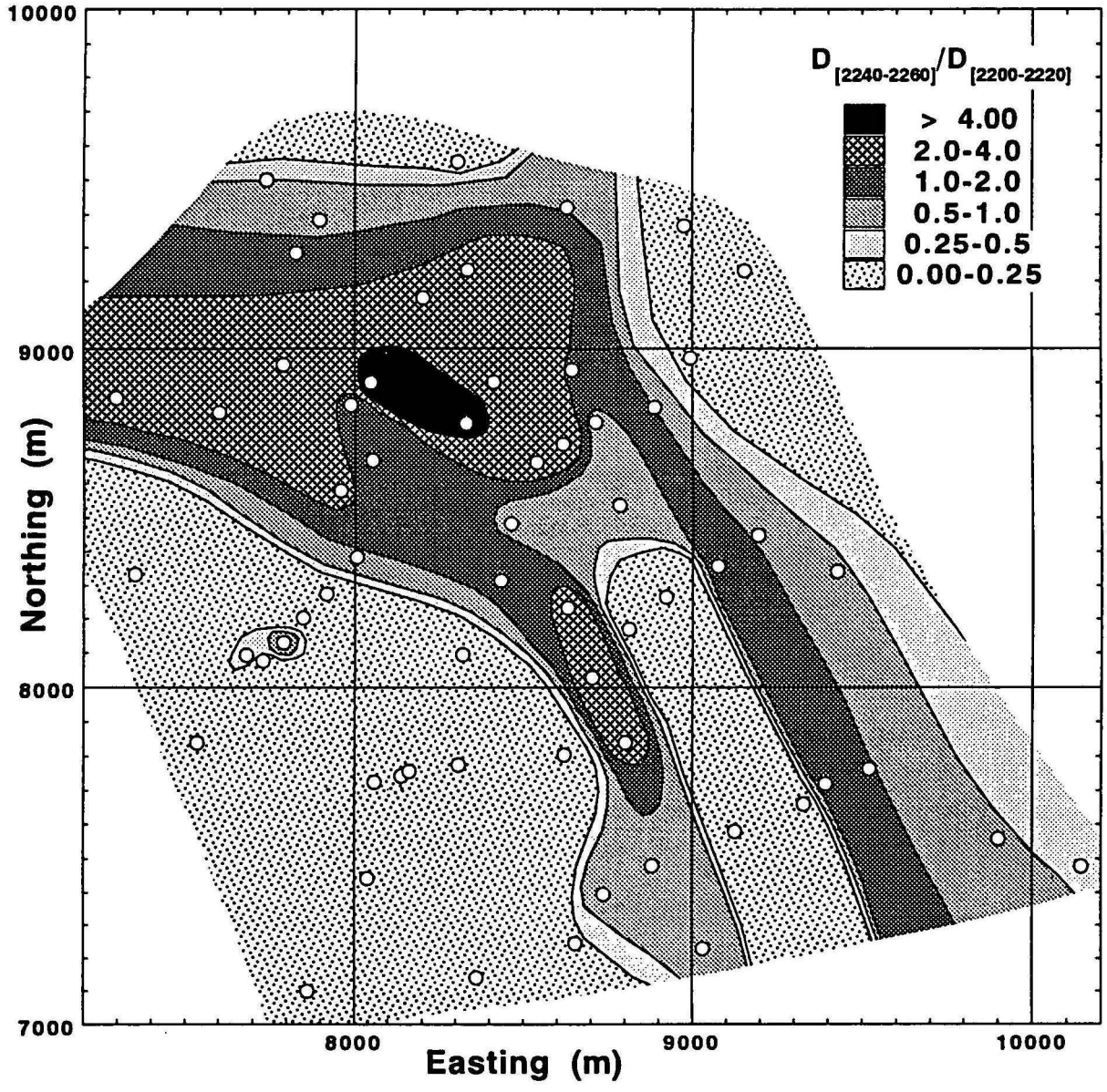

Figure 6. Spatial variations in depth ratio between the Fe-OH and Al-OH absorption peaks (e.g. $D_{[2240-2260]}/D_{[2200-2220]}$), Sulphur Springs area.

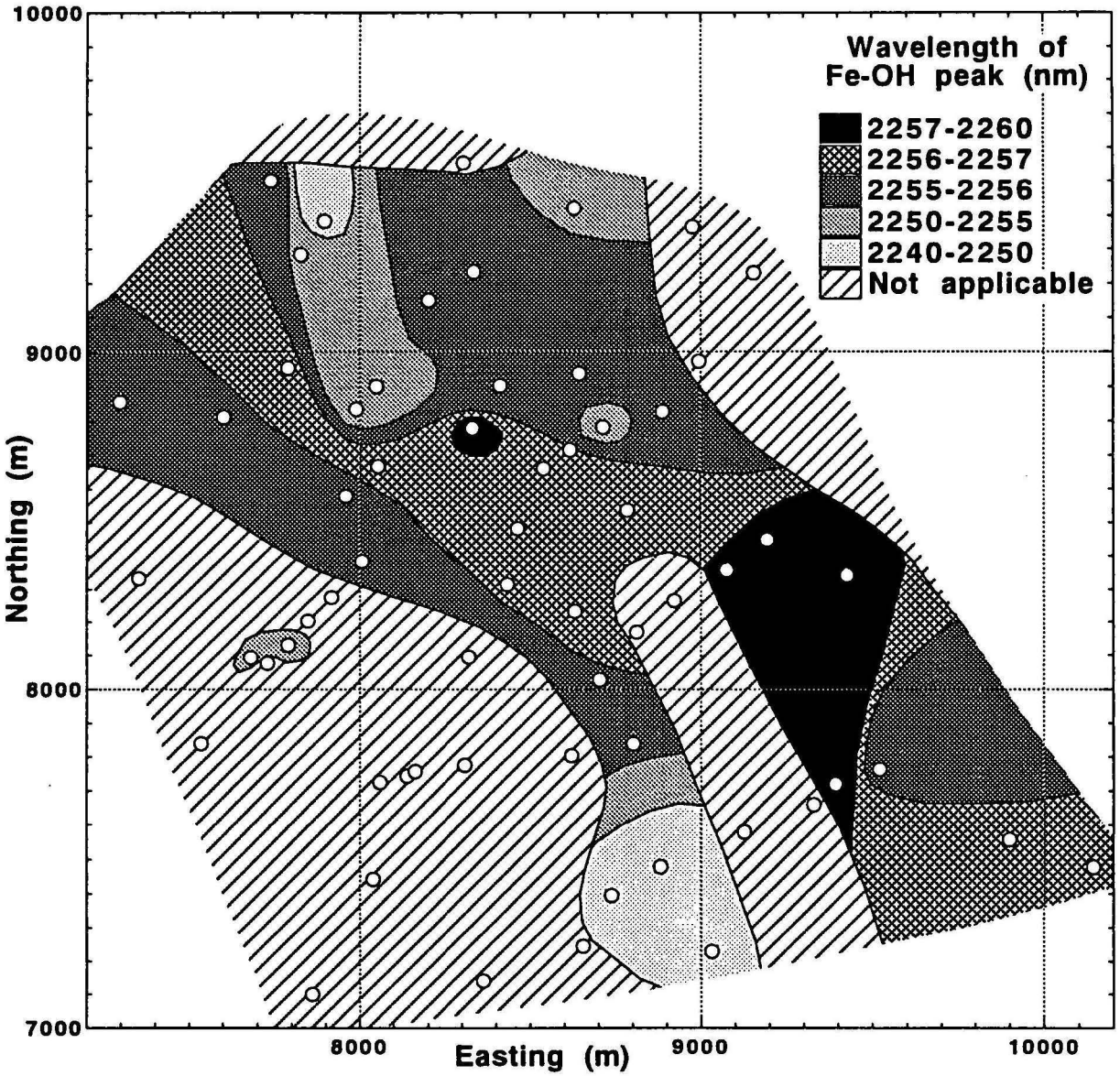

Figure 7. Spatial variations in the wavelength of the Fe-OH absorption peak, Sulphur Springs area.

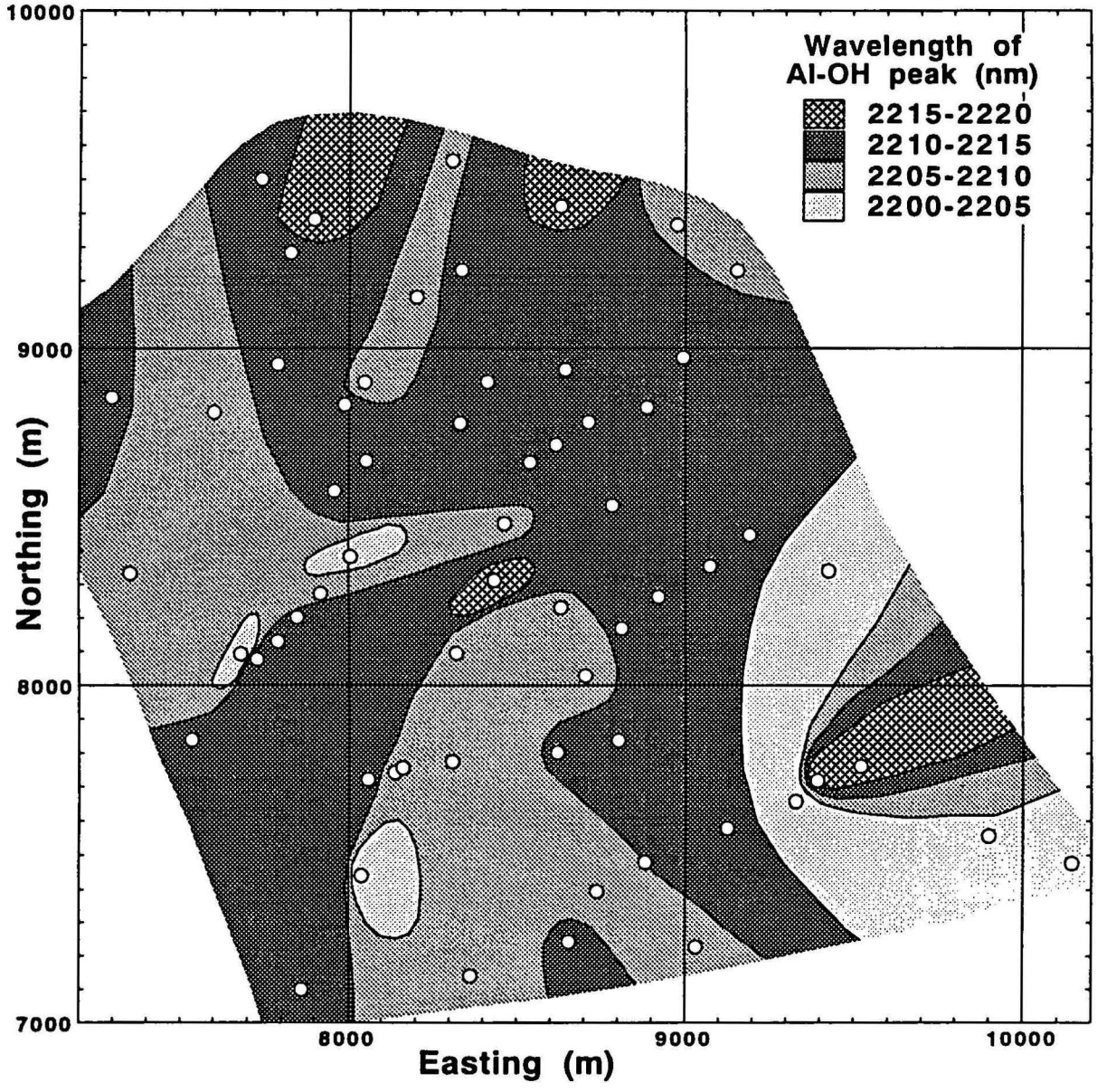

Figure 8. Spatial variations in the wavelength of the Al-OH absorption peak, Sulphur Springs area.

Table 2. Location, lithological characteristics, $\delta^{18}O$ and PIMA parameters of samples analysed in this study.

Sample	Easting (m)[1]	Northing (m)[1]	Lithology	Alteration assemblage	$\delta^{18}O$ (‰)	Spectral group	Wavelength of Fe-OH absorption peak	Wavelength of Fe-OH absorption peak	$\frac{D_{[2240-2260]}}{D_{[2200-2220]}}$
203310	8630	9420	dacite	chlorite-quartz	7.8	D	2219.6	2253.8	0.99
203315	8975	9365	dacite	sericite	9.8	A1	2206.4		0.00
203318	9155	9230	dacite	"background"	11.5	A1	2208.6		0.00
203320	8305	9555	dacite	sericite	9.8	A1	2209.0		0.00
203323	7740	9500	dacite	chlorite-quartz	10.6	A2	2210.8	2256.1	0.50
203332	7861	7100	equigranular granite	"background"	7.3	C	2212.4		0.00
203340	7353	8332	granophyre	"background"	7.6	C	2209.0		0.00
203349	8038	7441	granophyre	sericite	7.3	A1	2204.0		0.00
203350	8059	7723	granophyre	"background"	7.1	C	2211.4		0.00
207451	8137	7743	granophyre	"background"	7.5	C	2209.1		0.00
207452	8362	7142	granophyre	"background"	8.5	C	2209.6		0.00
207454	7536	7839	granophyre	sericite	8.1	A1	2211.7		0.00
207457	7681	8094	granophyre	chlorite-quartz	7.1	A2	2204.9	2252.0	0.42
207459	7796	5960	equigranular granite	"background"	6.6	C	2210.0		0.00
207493	8054	8668	andesite	chlorite-quartz	11.5	B1	2211.9	2256.3	1.92
207494	7789	8953	andesite	chlorite-quartz	5.0	B1	2211.9	2256.3	3.74
207495	7296	8855	felsic andesite	"background"	5.4	B1	2211.4	2255.8	2.70
207496	8922	8264	andesite	"background"	8.5	C	2210.7		0.00
207497	8006	8383	felsic andesite	chlorite-quartz	5.6	B3	2202.9	2255.5	0.87
207498	7917	8274	diorite	"background"	3.4	C	2208.3		0.00
207499	7847	8203	diorite-dolerite	"background"	1.1	C	2211.0		0.00
207501	7791	8130	diorite	"background"		B2	2213.4	2250.5	0.87
207502	7730	8076	pyroxenite	"background"	4.0	Other	2212.9		0.00
207503	8308	7775	diorite	"background"	3.2	C	2208.6		0.00
207504	8161	7756	diorite	"background"	5.3	C	2207.4		0.00
207505	8654	7244	diorite	"background"	5.3	C	2212.3		0.00
207506	8320	8095	diorite	"background"	5.1	C	2208.7		0.00
207101	8994	8972	andesite	sericite	10.3	A1	2209.3		0.00
207103	8631	8231	andesite	chlorite-quartz	5.0	B1	2207.9	2256.8	2.35
207104	8704	8028	andesite	chlorite-quartz	5.5	B1	2208.4	2255.9	2.27
207106	8802	7838	andesite	chlorite-quartz	5.2	B1	2212.2	2255.8	3.61
207109	8714	8781	dacite	chlorite-quartz	8.9	D	2214.0	2253.8	0.97
207110	8618	8715	andesite	chlorite-quartz	4.6	B1	2209.0	2256.0	2.80
207113	8540	8662	andesite	chlorite-quartz	4.7	B1	2211.0	2256.5	3.08
207114	8464	8481	andesite	chlorite-quartz	5.1	D	2205.8	2256.8	0.86
207117	8644	8937	andesite	chlorite-quartz	4.8	B1	2207.1	2255.5	1.83
207119	8412	8900	andesite	chlorite-quartz	4.2	B1	2210.9	2255.4	3.42
207121	8331	8778	andesite	chlorite-quartz	3.9	D		2258.2	
207125	7959	8579	felsic andesite	chlorite-quartz	4.8	B1	2211.2	2255.0	2.07
207129	8049	8900	andesite	chlorite-quartz	3.8	B1	2207.4	2253.0	4.17
207131	7989	8833	andesite	"background"	3.9	D	2210.7	2250.1	0.97
207134	8336	9232	andesite	chlorite-quartz	5.4	B1	2210.4	2255.2	3.35
207135	8202	9151	andesite	chlorite-quartz	1.5	B1	2209.6	2255.6	2.91
207143	7601	8811	felsic andesite	chlorite-quartz	3.9	B1	2207.6	2255.9	3.84
207145	7826	9284	andesite	"background"	5.0	B1	2212.8	2252.8	1.46
207146	7897	9382	andesite	"background"	2.2	A2	2216.8	2249.2	0.63
207161	8887	8825	andesite	"background"	8.3	B2	2212.4	2255.5	1.00
207163	8784	8535	andesite	"background"	7.5	B2	2213.0	2256.5	0.87
207164	8812	8169	andesite	"background"	6.8	C	2210.4		0.00
207165	9075	8355	andesite	"background"	8.6	B2	2208.0	2258.2	1.17
207166	9194	8447	andesite	"background"	9.1	B2	2209.0	2257.9	0.96
207167	9427	8341	andesite	"background"	11.2	B3	2201.7	2257.8	0.62
207175	8434	8313	andesite	chlorite-quartz	5.6	D	2219.2	2256.1	1.40
207176	9126	7579	andesite	"background"	7.0	C	2210.4		0.00
207177	9329	7659	andesite	"background"	7.6	Other	2202.7		0.00
207178	9393	7719	andesite	"background"	7.5	B1	2215.9	2257.3	1.84
207179	9521	7761	andesite	"background"	9.0	B2	2217.5	2255.8	1.02
207181	9900	7557	andesite	"background"	10.7	B3	2204.8	2256.2	0.88
207192	8621	7803	felsic andesite	"background"	5.0	C	2211.2		0.00
207195	8881	7480	felsic andesite	"background"	5.3	D	2210.0	2247.1	0.73
207196	8737	7394	felsic andesite	"background"	5.0	D	2208.6	2246.4	0.84
207198	9031	7229	andesite	chlorite-quartz	5.8	D	2205.5	2242.0	0.78
207238	10142	7476	dacite	"background"	12.7	A2	2200.9	2256.9	0.33

[1]The reference point for the grid is AMG coordinates 7650000N and 720000E

Wavelength variation of the Al-OH absorption band. Variations in the wavelength of the Al-OH absorption band (2180-2220) can be used as a qualitative guide to the composition of sericite. Paragonite has a characteristic absorption band at 2188 nm; muscovite has an absorption band at 2202 nm; and phengite has an absorption band at 2220 nm (Pontual and Merry, 1995). Inspection of Figure 8 indicates that most samples have an Al-OH absorption peak of between 2205 and 2215 nm, which suggests that the main sericite mineral present tends to phengitic muscovite. However, there is no systematic spatial variation in the data.

Measured spectral responses and $\delta^{18}O$: inter-correlations

In addition to determining spatial variations in the measured PIMA parameters, these data were compared with each other and with whole rock $\delta^{18}O$ data on scattergrams (Figs. 9 to 13). The PIMA parameters were plotted against $\delta^{18}O$ as $\delta^{18}O$ is strongly dependant on the temperature of alteration and on relative mineral abundances. The samples were grouped and plotted according to the alteration assemblage.

Chlorite-quartz alteration assemblage. For most chlorite-quartz altered samples, the Fe-OH absorption peak is restricted to a narrow range of 2255-2257 nm, indicating Fe-rich chlorite. Against $D_{[2240\text{-}2260]}/D_{[2200\text{-}2220]}$, which is a rough guide to chlorite/sericite ratios, the Fe-OH absorption peak plots as a vertical array, which implies that chlorite composition is independant of relative chlorite abundance (Fig. 9). However, the Fe-OH absorption peak has a weak negative correlation with whole rock $\delta^{18}O$, which suggests that the composition of chlorite may be, in part, dependant on the temperature of chlorite-quartz alteration. No systematic correlation was noted between the Fe-OH and Al-OH absorbance peaks.

On a $\delta^{18}O$ versus Al-OH absorption peak scattergram (Fig. 11), chlorite-quartz altered samples can be split into two groups: (a) samples with low $\delta^{18}O$ and Al-OH peaks, and (b) samples with high $\delta^{18}O$ and Al-OH absorption peaks. Group (a) consists mostly of andesitic rocks, whereas the majority of goup (b) consists of dacitic rocks. Both groups show a negative correlation between $\delta^{18}O$ and the Al-OH absorption peak (Fig. 11). These groups are also apparent when the Al-OH absorption peak is plotted against $D_{[2240\text{-}2260]}/D_{[2200\text{-}2220]}$ (Fig. 12). Group (a) samples display a strong positive correlation between Al-OH absorption peak and $D_{[2240\text{-}2260]}/D_{[2200\text{-}2220]}$, suggesting that more phengitic sericite occurs in samples with higher chlorite/sericite ratios. Group (b) samples have lower $D_{[2240\text{-}2260]}/D_{[2200\text{-}2220]}$ ratios, and lack correlation.

For samples with $\delta^{18}O$ below 6‰, which roughly corresponds with group (a), $D_{[2240\text{-}2260]}/D_{[2200\text{-}2220]}$ is negatively correlated with whole rock $\delta^{18}O$ (Fig. 13). This relationship suggests that relative chlorite abundances exert a strong influence on whole rock $\delta^{18}O$: chlorite-rich samples have low $\delta^{18}O$. This observation is consistent with expected variation as of all the abundant alteration minerals, chlorite concentrates ^{18}O least effectively (e.g. Taylor, 1979). Group (b) samples are not correlated on this diagram.

Sericite-dominant alteration assemblage. Samples characterised by sericite-dominant alteration assemblages, which are present mainly in the dacite and parts of the Strelley Granite, lack Fe-OH absorption peaks; therefore, the samples do not plot on Figures 9 and 10. On Figure 12 and 13, these samples plot along the abscissa, with $D_{[2240\text{-}2260]}/D_{[2200\text{-}2220]}$ equal to zero. In Figure 11, which plots the Al-OH absorption peak versus $\delta^{18}O$, no systematic variations were observed.

"Background" alteration assemblage. "Background" (e.g. chlorite-quartz-albite±carbonate±pyrite) altered samples form a field on the Fe-OH absorption peak versus $D_{[2240\text{-}2260]}/D_{[2200\text{-}2220]}$ diagram (Fig. 9) that is characterised by $D_{[2240\text{-}2260]}/D_{[2200\text{-}2220]} \sim 0.5\text{-}1.0$ when

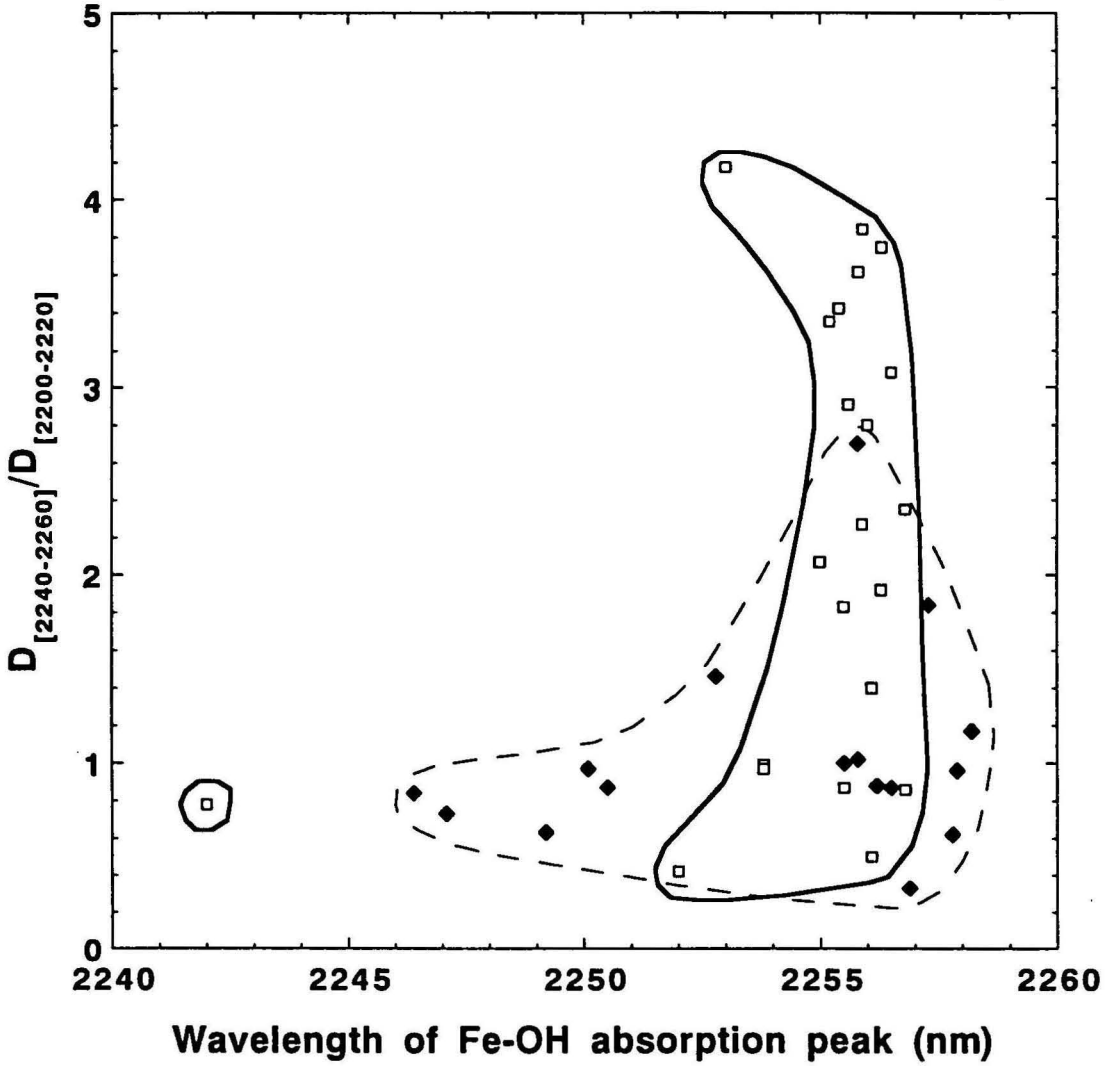

Figure 9. Scattergram showing the relationship between the Fe-OH absorption peak and $D_{[2240\text{-}2260]}/D_{[2200\text{-}2220]}$. Solid diamonds indicate "background" altered samples; and open squares indicate chlorite-quartz altered samples.

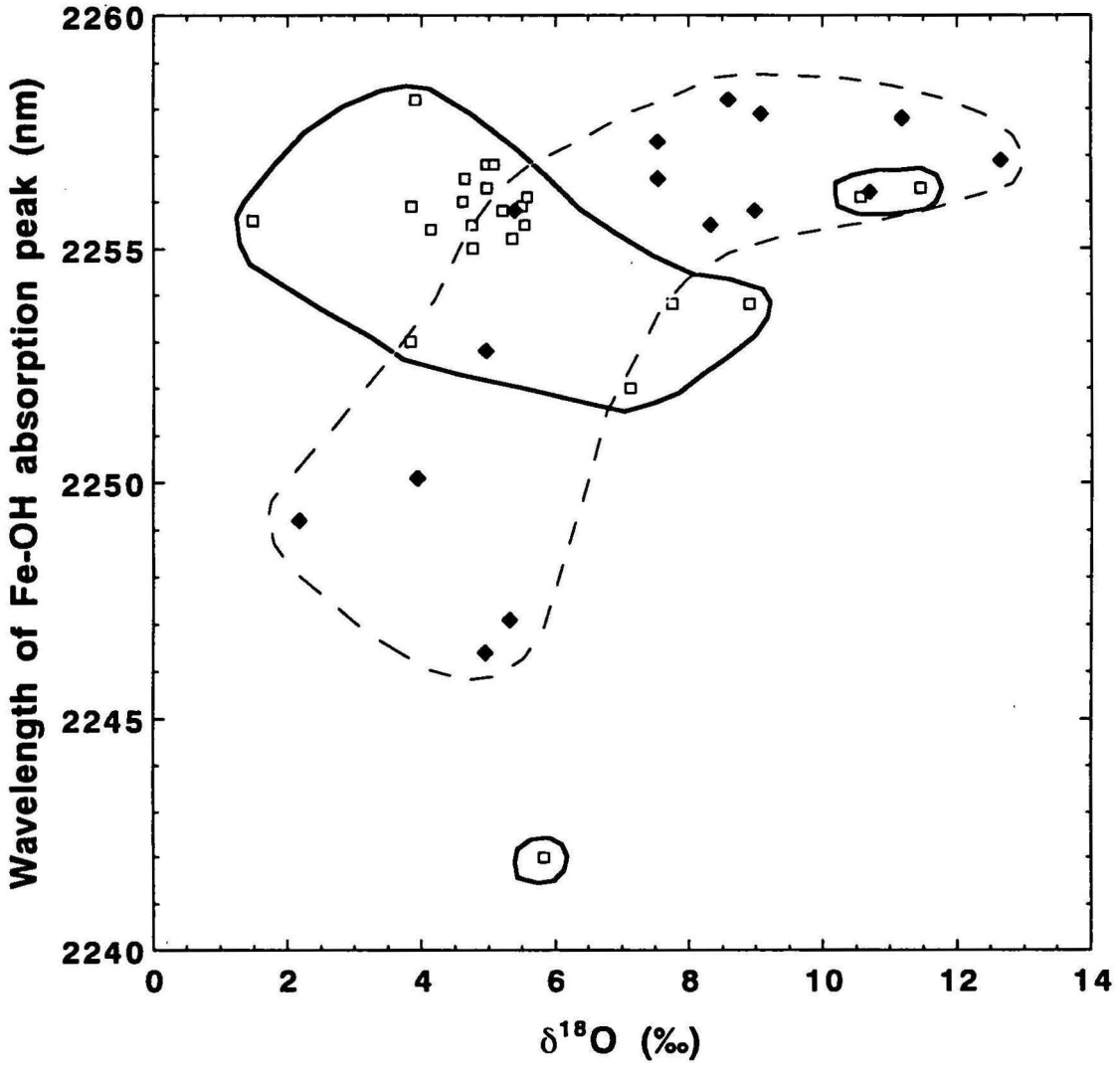

Figure 10. Scattergram showing the relationship between $\delta^{18}O$ and the Fe-OH absorption peak. Solid diamonds indicate "background" altered samples; and open squares indicate chlorite-quartz altered samples.

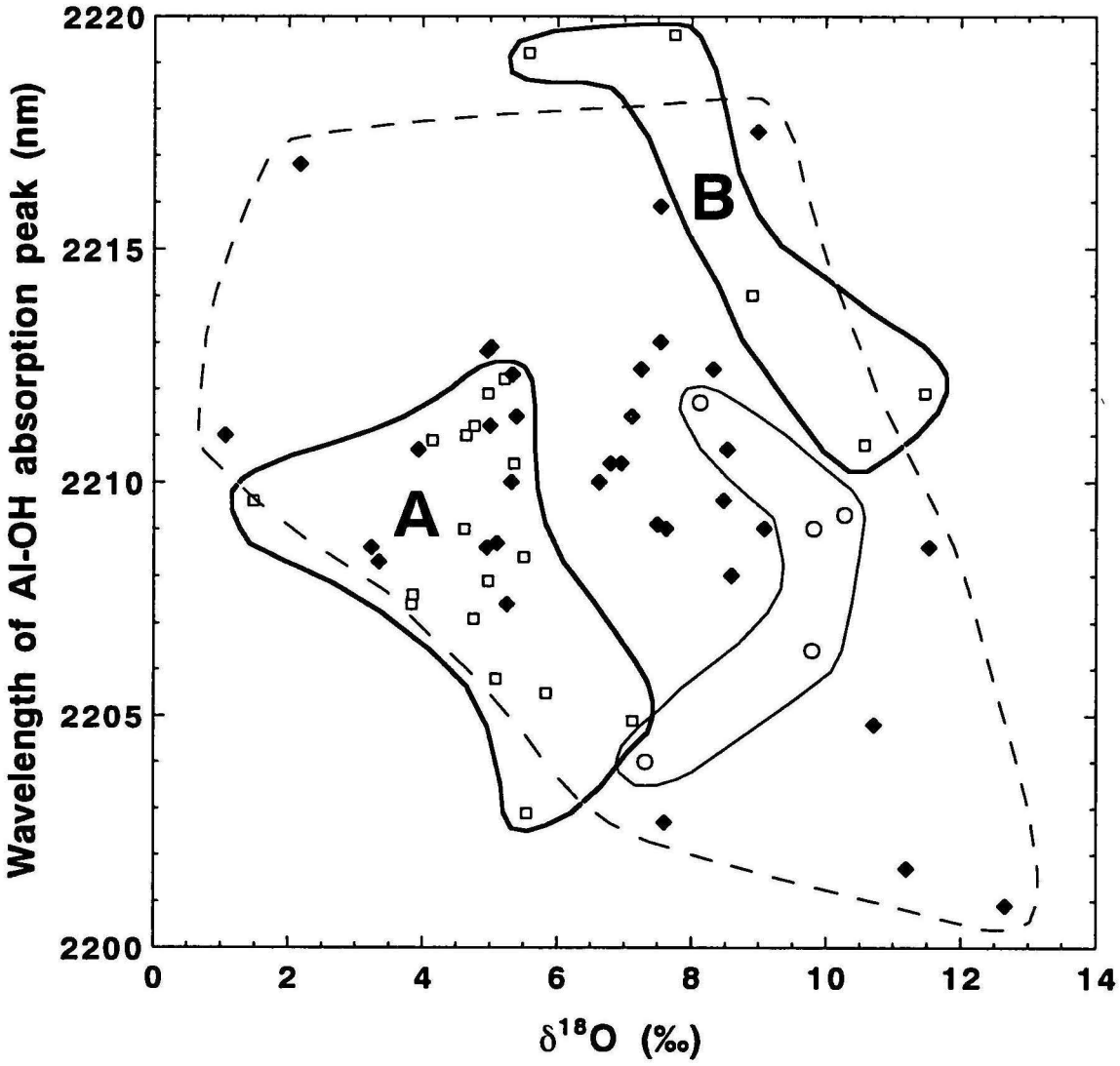

Figure 11. Scattergram showing the relationship between $\delta^{18}O$ and the Al-OH absorption peak. Solid diamonds indicate "background" altered samples; open circles indicate sericite altered samples; and open squares indicate chlorite-quartz altered samples.

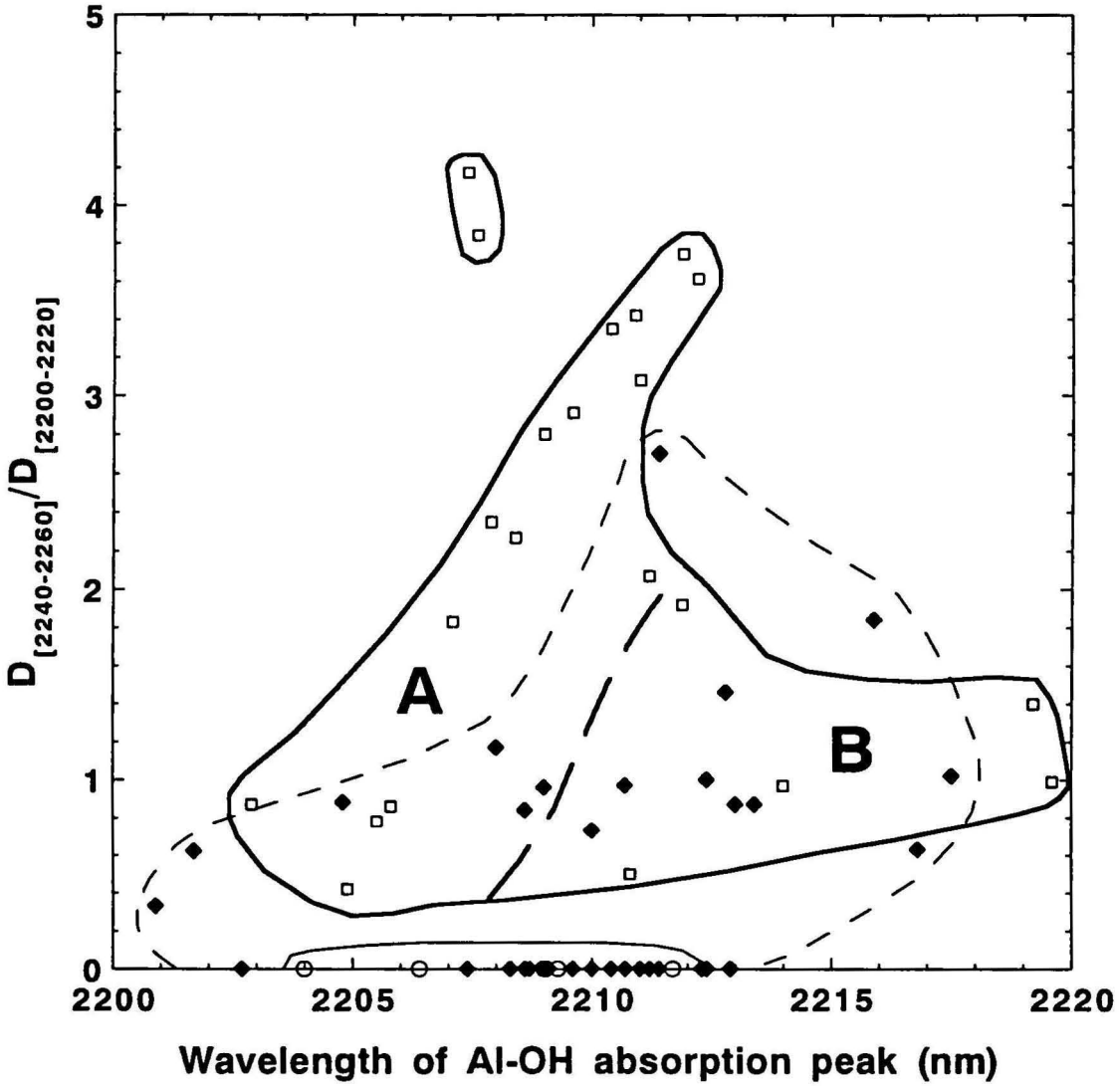

Figure 12. Scattergram showing the relationship between the Al-OH absorption peak and $D_{[2240\text{-}2260]}/D_{[2200\text{-}2220]}$. Solid diamonds indicate "background" altered samples; open circles indicate sericite altered samples; and open squares indicate chlorite-quartz altered samples.

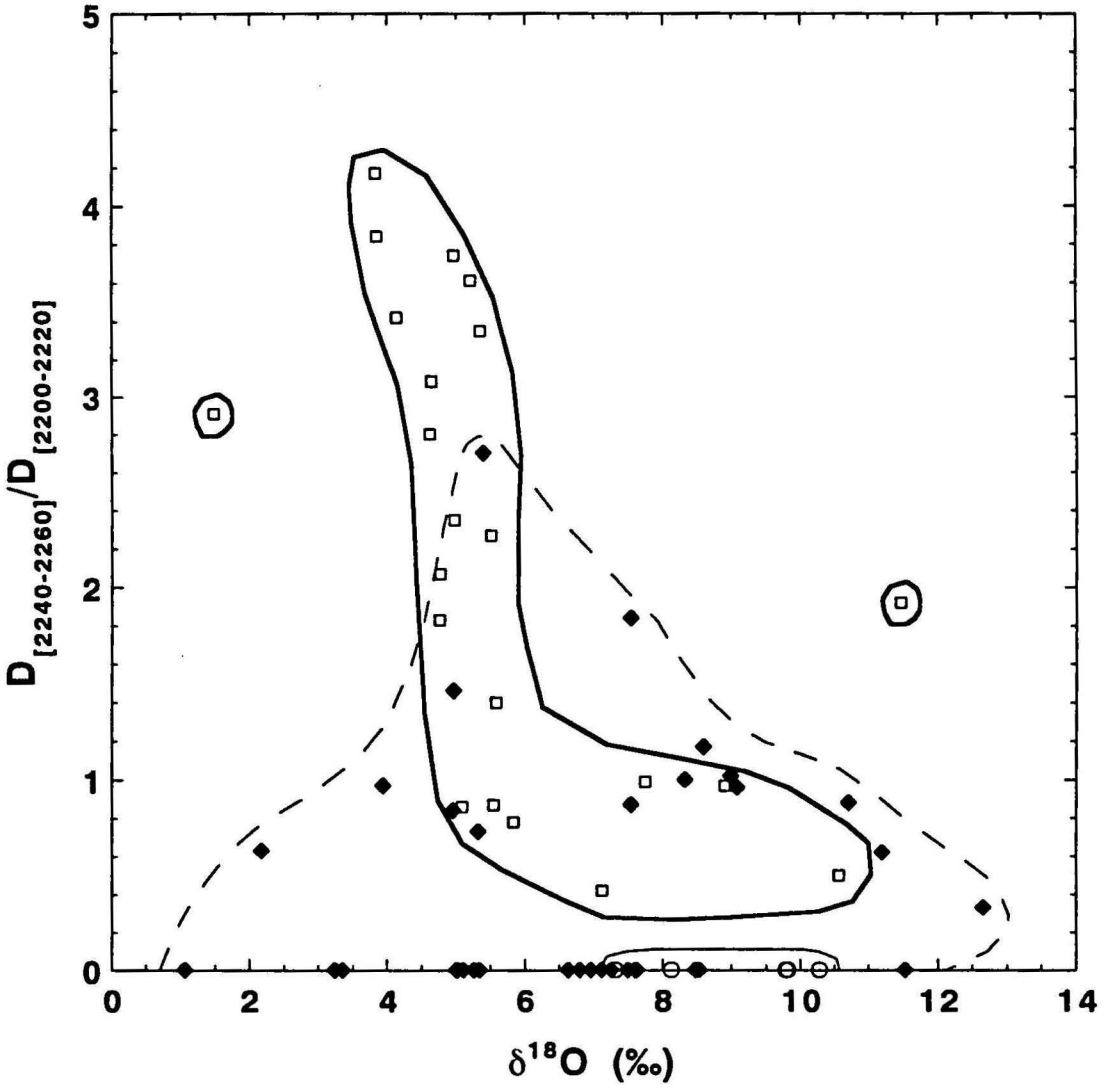

Figure 13. Scattergram showing the relationship between the $\delta^{18}O$ and $D_{[2240-2260]}/D_{[2200-2220]}$. Solid diamonds indicate "background" altered samples; open circles indicate sericite altered samples; and open squares indicate chlorite-quartz altered samples.

the Fe-OH absorption peak is less than 2253 nm. Above 2253 nm, this trend curves into the vertical trend defined by chlorite-quartz-altered samples.

A strong positive correlation is noted between $\delta^{18}O$ and the Fe-OH absorption peak for "background" altered samples. This contrasts with the weak negative correlation observed for chlorite-quartz-altered samples (Fig. 10). A broad negative correlation betwen the Al-OH absorption peak and $\delta^{18}O$ is present (Fig. 11), but no significant correlation is noted between $D_{[2240\text{-}2260]}/D_{[2200\text{-}2220]}$ and the Al-OH absorption peak (Fig. 12) or $\delta^{18}O$ (Fig. 13).

Geological significance, exploration applications and further work

Based on the above results, certain characteristics of PIMA spectra have potential as exploration guides in defining the extent and type of alteration associated with VHMS deposits. In addition, these same parameters can be used to understand processes by which alteration zones in VHMS districts form. Relatively unsophisticated treatment of the spectra indicate that $D_{[2240\text{-}2260]}/D_{[2200\text{-}2220]}$ and the wavelength of the Fe-OH absorption peak can be used directly as exploration guides and vectors. Although the wavelength of the Al-OH absorption peak does not show systematic spatial vatiation with alteration, correlation with other parameters indicate that it may be useful in understanding the genesis of alteration.

Geological significance of the $D_{[2240\text{-}2260]}/D_{[2200\text{-}2220]}$ ratio

The depth ratio of the Fe-OH to Al-OH peaks was calculated as an indication of chlorite/sericite ratios. At this writing, $D_{[2240\text{-}2260]}/D_{[2200\text{-}2220]}$ is only a qualitative guide to the chlorite/sericite ratio for three reasons: (1) lack of calibration, (2) effects of chlorite composition on the depth of the Fe-OH absorption peak, and the effects of sericite crystallinity on the depth of the Al-OH absorption peak. Calibration of $D_{[2240\text{-}2260]}/D_{[2200\text{-}2220]}$ is the subject of ongoing research, but some preliminary generalisations may be made by comparing PIMA data to petrographic and geochemical data.

At face value, $D_{[2240\text{-}2260]}/D_{[2200\text{-}2220]}$ values near zero suggest that a sample has abundant sericite and lacks chlorite. However, several "background" altered samples, in which chlorite is a characteristic mineral, have $D_{[2240\text{-}2260]}/D_{[2200\text{-}2220]}$ of zero. Petrographic examination and geochemical analyses of these samples confirm the presence of chlorite in these samples as a major component. Sericite is also present, but in abundances less than that of chlorite. Hence, either $D_{[2240\text{-}2260]}/D_{[2200\text{-}2220]}$ does not reflect chlorite/sericite ratios, or the spectral response of sericite is much greater than that of chlorite.

Variations in relative chlorite and sericite abundances are a common occurrence in many VHMS districts. In most cases, chlorite is enriched in alteration zones proximal to deposits, whereas sericite is enriched distal to deposits (c.f. Franklin et al., 1981) The PIMA results at Sulphur Springs are consistent with this generalisation: high $D_{[2240\text{-}2260]}/D_{[2200\text{-}2220]}$ values occur in a pipe underlying the Sulphur Springs deposit, whereas lower values occur lateral to this pipe. This zonation occurs over the scale of a kilometre or more, which suggests that this ratio can be used as semi-regional exploration guide.

Geological significance of the Fe-OH absorbance peak

Spatial variations in the Fe-OH absorbance peak (Fig. 7)indicate that the alteration pipe underlying the Sulphur Springs is characterised by values of between 2255 and 2257 nm. Qualitatively this indicates Fe-rich chlorite. Zones characterised by lower values for the Fe-OH absorbance peak, which indicate more Mg-rich chlorite, occur in the peripheral parts

of the chlorite-quartz alteration zone and in the "background" alteration zone west and southeast of the Sulphur Springs deposit. The occurrence of more Mg-rich chlorite in peripheral parts of chloritic alteration zones has also been observed in the Noranda, Quebec district (Riverin, 1977). These data suggest that variations in the Fe-OH absorbance peak can be used to constrain peripheral parts of chlorite-quartz alteration zones.

Exploration applications

In the Panorama district, Brauhart (1997), and Brauhart and Morant (1997) have demonstrated the efficacy of regional alteration mapping as an exploration tool in well exposed terraines. This study essentially confirms the results of the alteration mapping. In particular, variations in $D_{[2240\text{-}2260]}/D_{[2200\text{-}2220]}$ effectively map changes in alteration assemblages defined by alteration mapping. Variations in $D_{[2240\text{-}2260]}/D_{[2200\text{-}2220]}$ and the Fe-OH absorbance peak may define subtle changes in alteration not defined by mapping (e.g. strataform zone of high $D_{[2240\text{-}2260]}/D_{[2200\text{-}2220]}$ present in the upper part of "background" altered andesite southeast of Sulphur Springs). In poorly exposed terrains, PIMA analyses may prove superior to alteration mapping in defining alteration zonation, particularly if RAB chips are available.

As PIMA analyses are rapid (collection of the 63 spectra in this study took less than one day), and consequently inexpensive, this technique has significant advantages over methods such as whole rock and isotope geochemistry. *However, the interpretation of the data requires a more sophisticated knowledge of local alteration mineralogy to be effective.*

Further work

Preliminary studies around the Sulphur Springs deposit indicate that the PIMA has potential both as an exploration tool and as a method of studying ore genesis. Further PIMA work on the Panorama area should include: (1) more detailed analysis of existing PIMA spectra(e.g. sericite crystallinity, kaolinite presence), (2) a more rigorous analysis of the geological significance of some of the parameters measured by the PIMA, (3) a comparison of spectra derived from powders with those derived from hand samples, and (4) an extension of the study to cover the whole Strelley Sequence. An important aspect of the last item is determining if chlorite-quartz altered rocks can be distinguished from background altered rocks in strongly weathered dacite. In addition, the relationship of $D_{[2240\text{-}2260]}/D_{[2200\text{-}2220]}$ to chlorite/sericite ratios and that of the Fe-OH absorption peak to chlorite composition must be calibrated.

Conclusions

This study has demonstrated that PIMA analysis has great potential as an exploration tool and in determining the genesis of VHMS deposits. The $D_{[2240\text{-}2260]}/D_{[2200\text{-}2220]}$ ratio, which is designed to reflect chlorite/sericite ratios, very effectively maps out the zone of chlorite-quartz alteration below the Sulphur Springs deposit. The major difficulty to using the PIMA quantitatively is the lack of calibration of PIMA parameters to mineral abundance and composition.

References

Brauhart, C., 1996, Preliminary report on alteration mapping of the Strelley Volcanic Sequence: Unpublished University of Western Australia report, 8 p.

Brauhart, C., 1997, The geology of the Strelley Granite and its role as subvolcanic heater to overlying VMS systems; Geological Society of Australia Abstracts, v. 44, p. 14.

Brauhart, C., and Morant, P., 1997, Regional alteration systems about VMS mineralisation at Panorama, Pilbara Block, Western Australia, v. 44, p. 15.

Franklin, J.M., Sangster, D.M., and Lydon, J.L., 1981, Volcanic-associated massive sulfide deposits: Economic Geology 75th Anniversary Volume, p. 485-627.

Morant, P., 1995, The Panorama Zn-Cu VMS deposits, Western Australia: AIG Bulletin, v. 16, p. 75-84.

Pontual, S., and Merry, N., 1995, PIMA workshop 2: practical implementation of the PIMA in exploration and mining: Unpublished workshop notes, 38 p.

Riverin, G., 1977, Wall-rock alteration at the Millenbach mine, Noranda area, Quebec: Unpublished Ph.D. thesis, Queen's University, Kingston, Ontario, 255 p.

Taylor, H.P., Jr., Oxygen and hydrogen isotope relationships in hydrothermal minerals deposits, in Barnes, H.L., ed., Geochemistry of hydrothermal ore deposits, second edition: Wiley, New York, p. 236-277.

Appendix: PIMA spectra for 63 samples from the Sulphur Springs area, Panorama district, central Pilbara, Western Australia

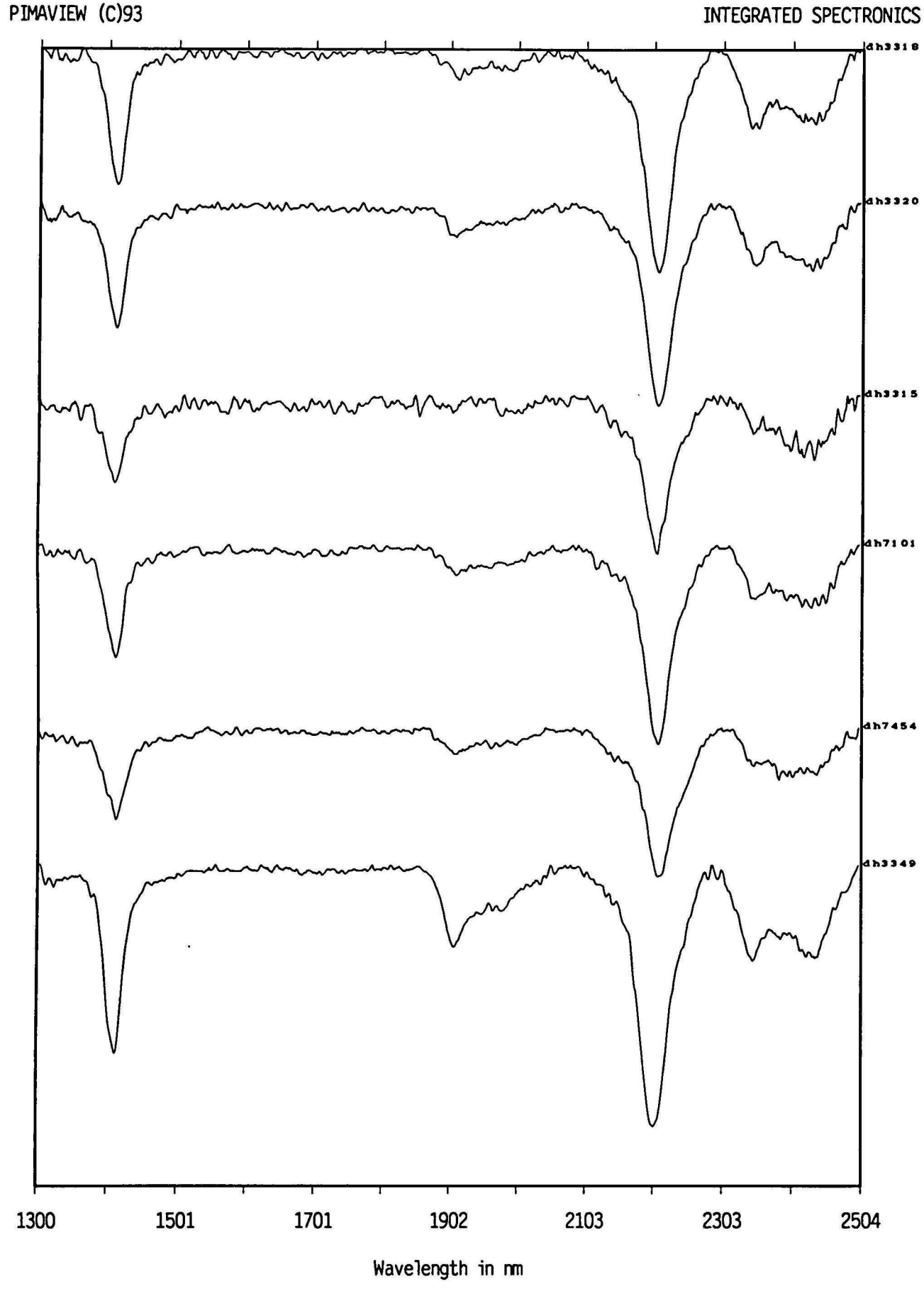

Sulphur Springs group A1

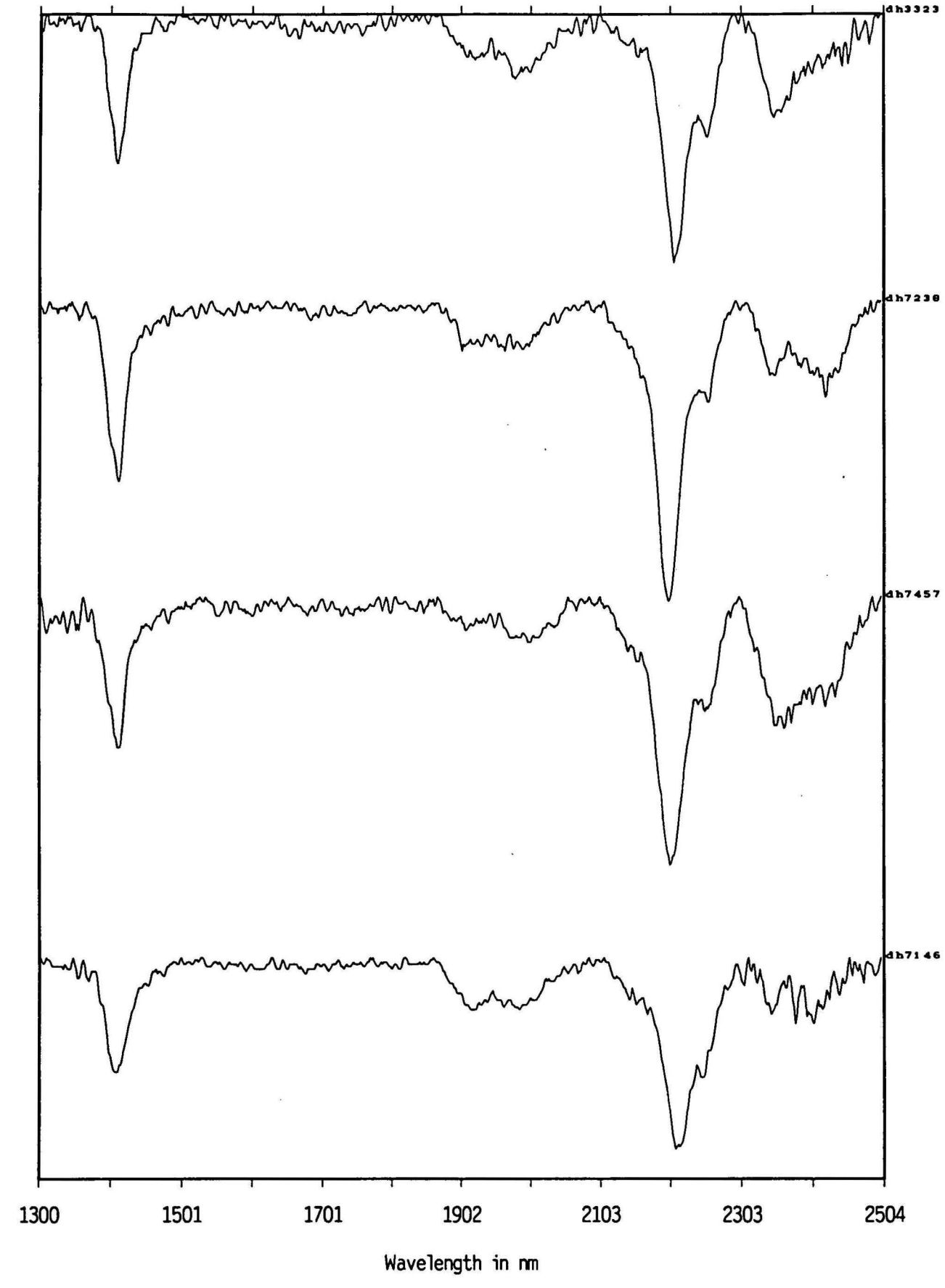

Sulphur Springs group A2

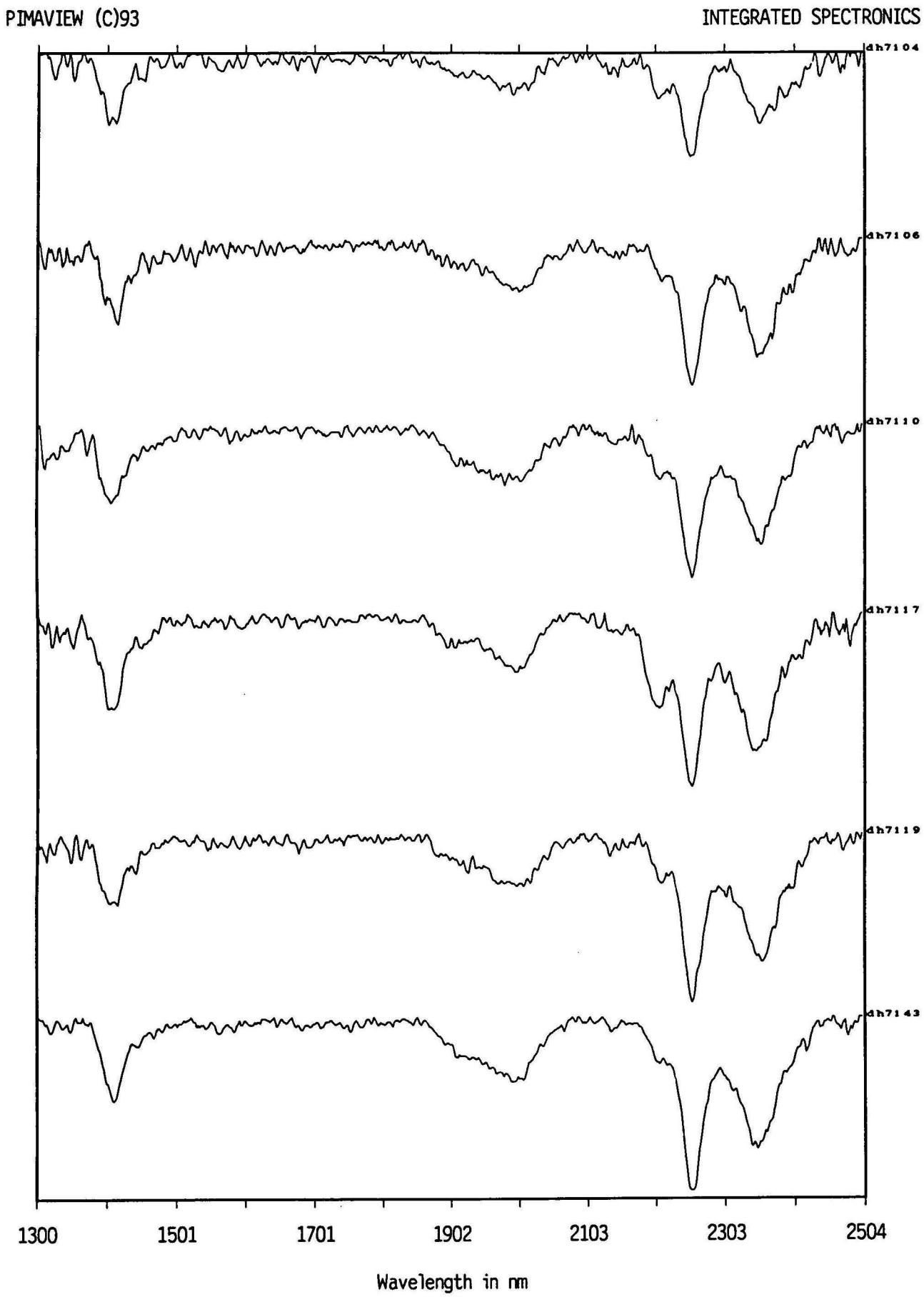

Sulphur Springs group B1

PIMAVIEW (C)93 INTEGRATED SPECTRONICS

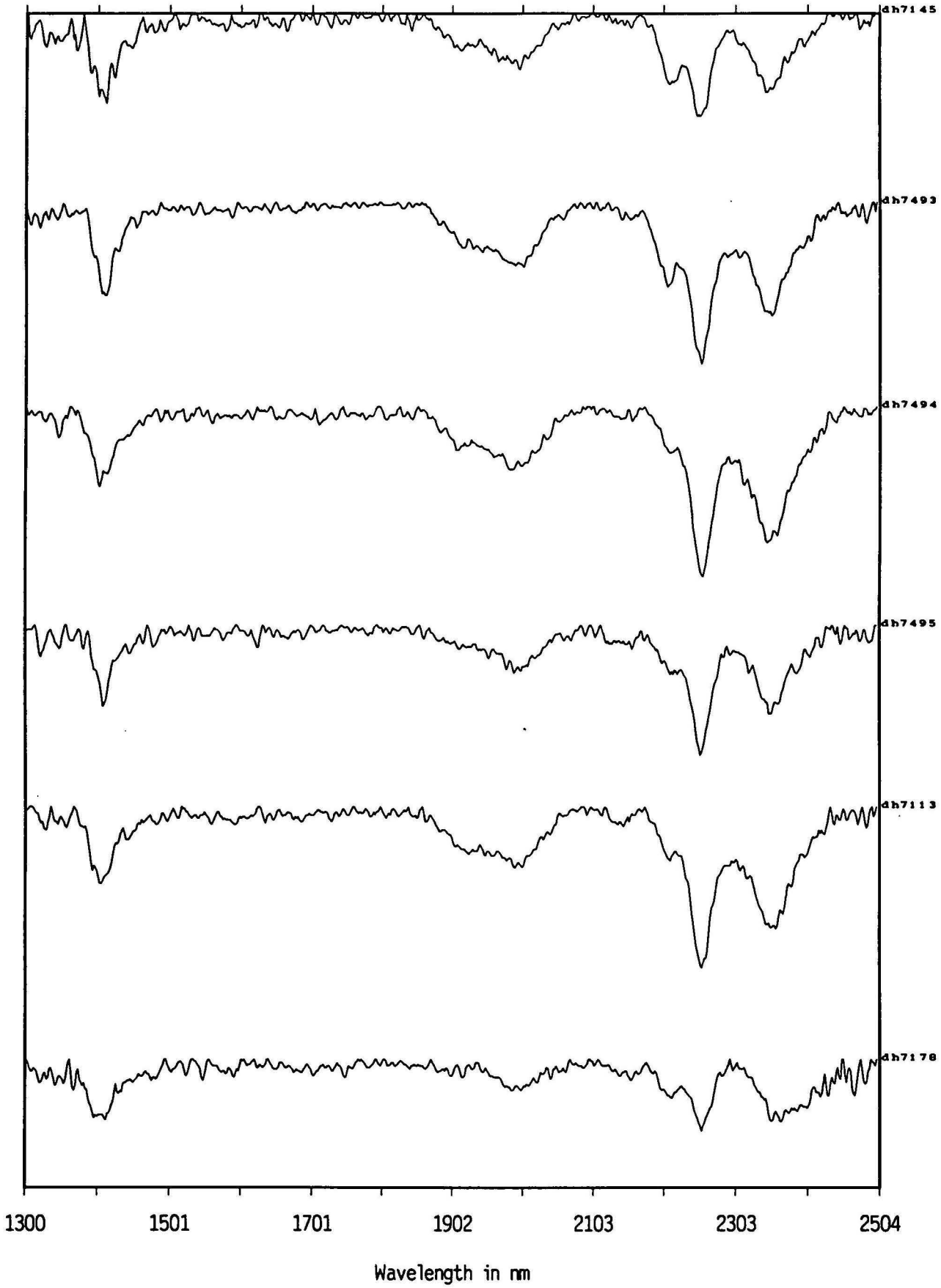

Sulphur Springs group B1

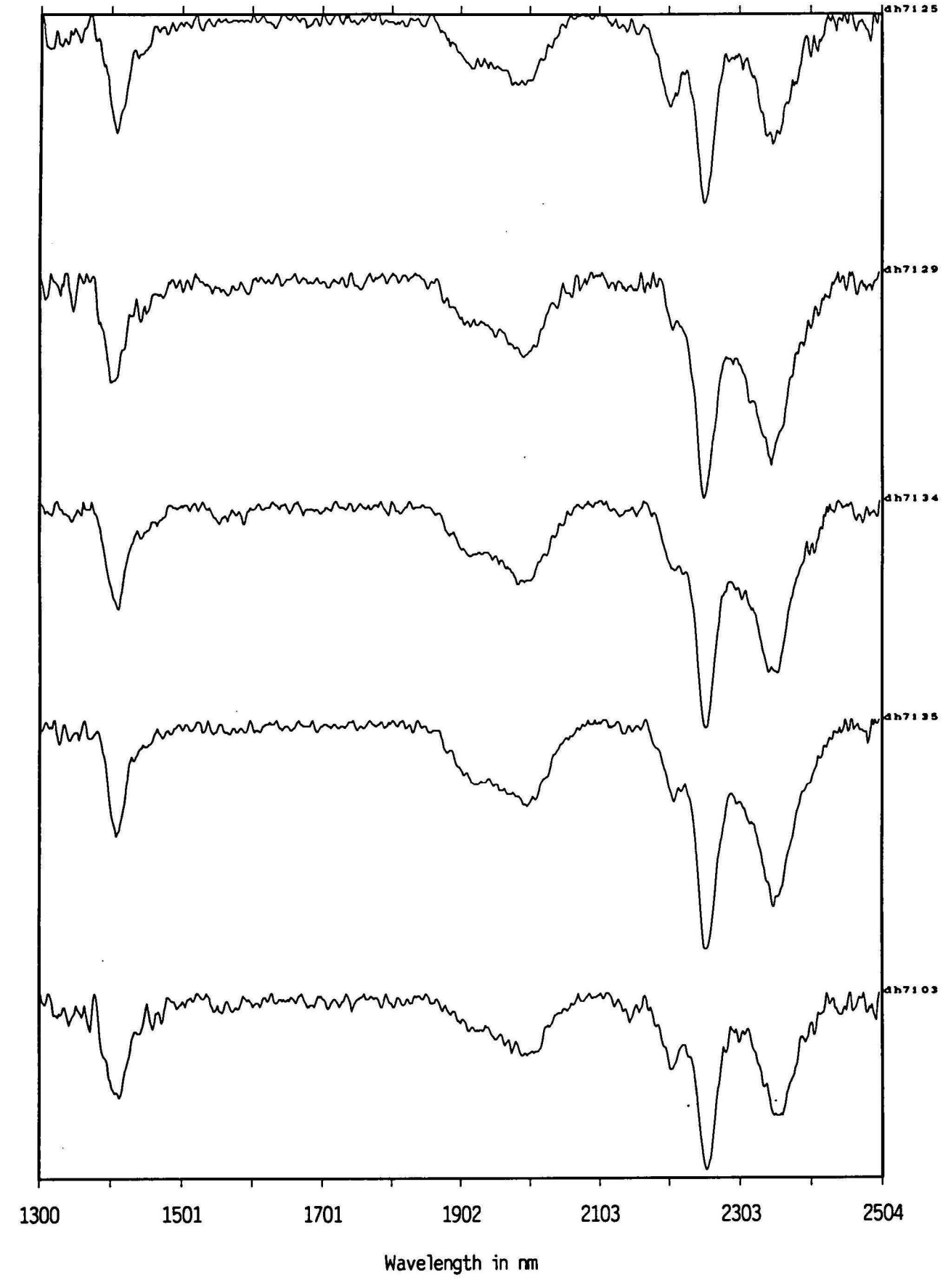

Sulphur Springs group B1

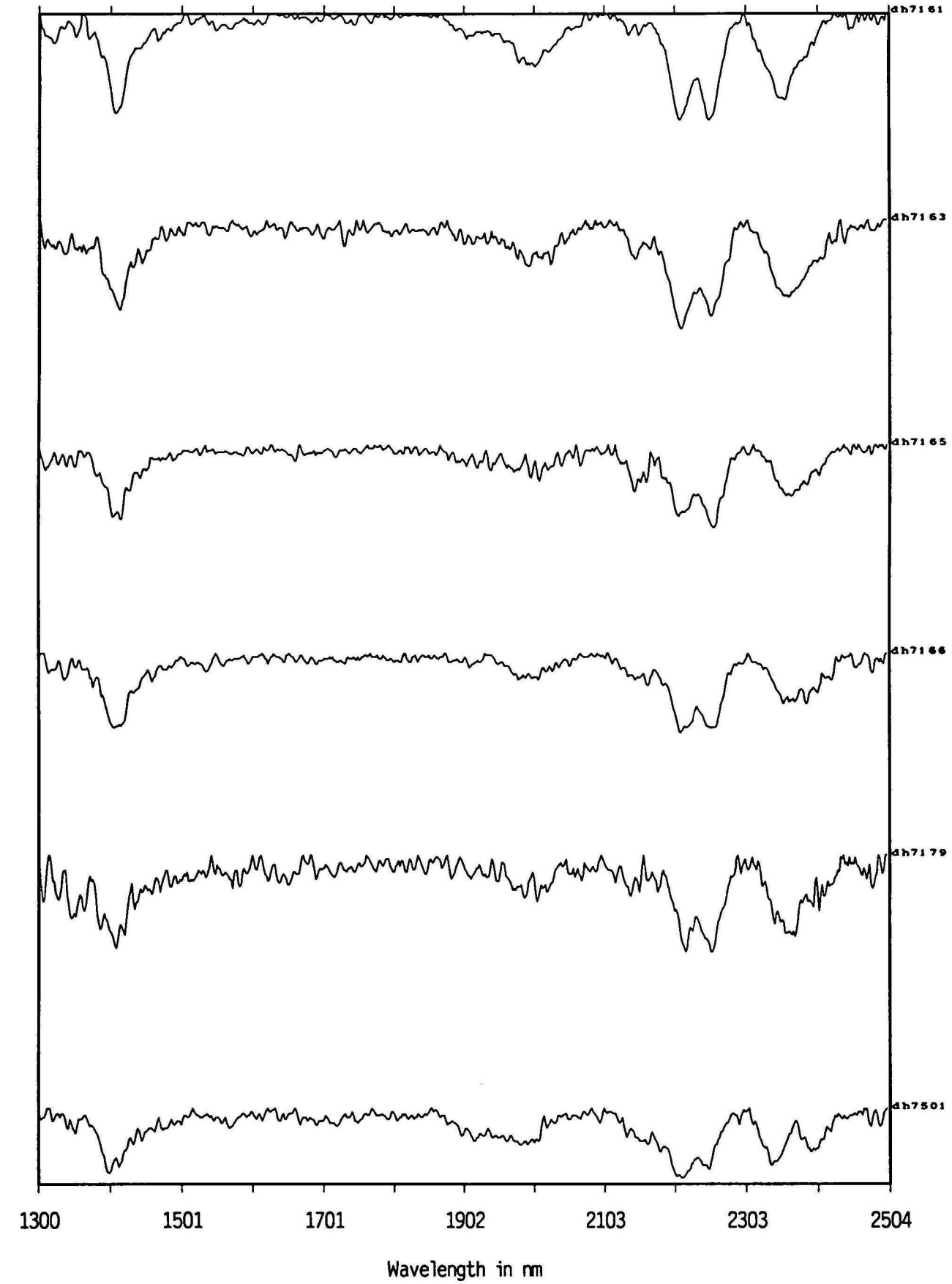

Sulphur Springs group B2

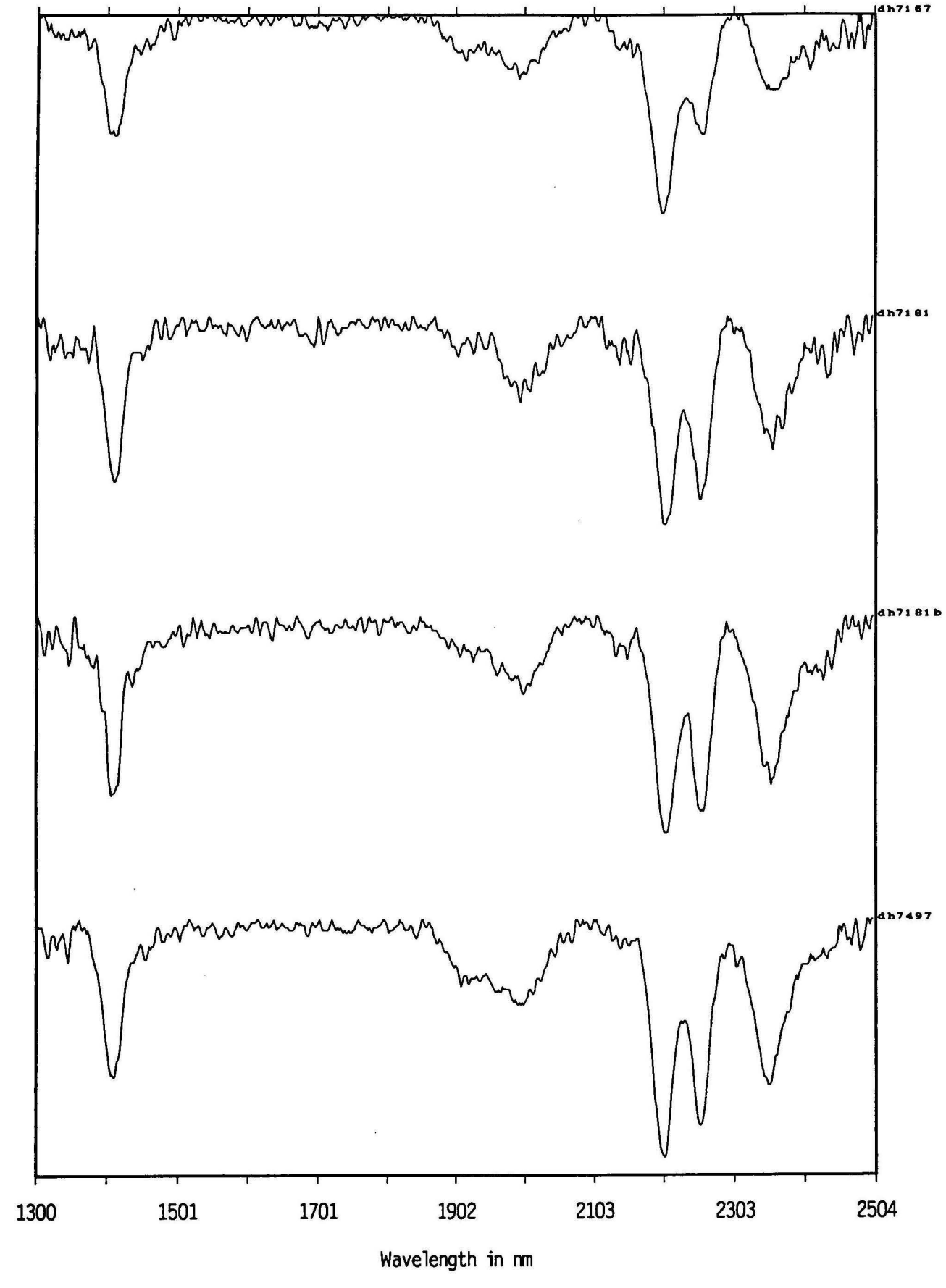

Sulphur Springs group B3

PIMAVIEW (C)93 INTEGRATED SPECTRONICS

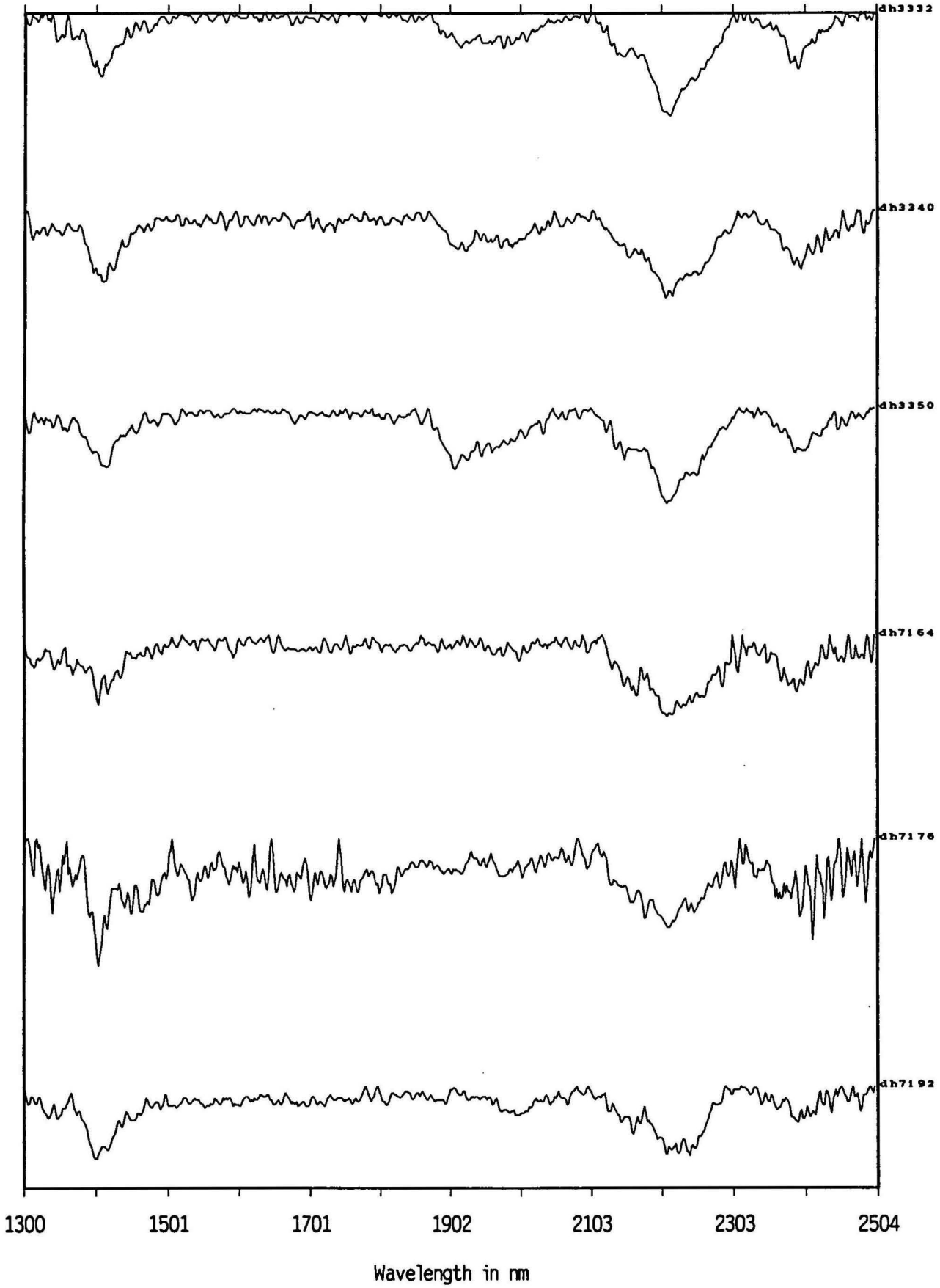

Sulphur Springs group C

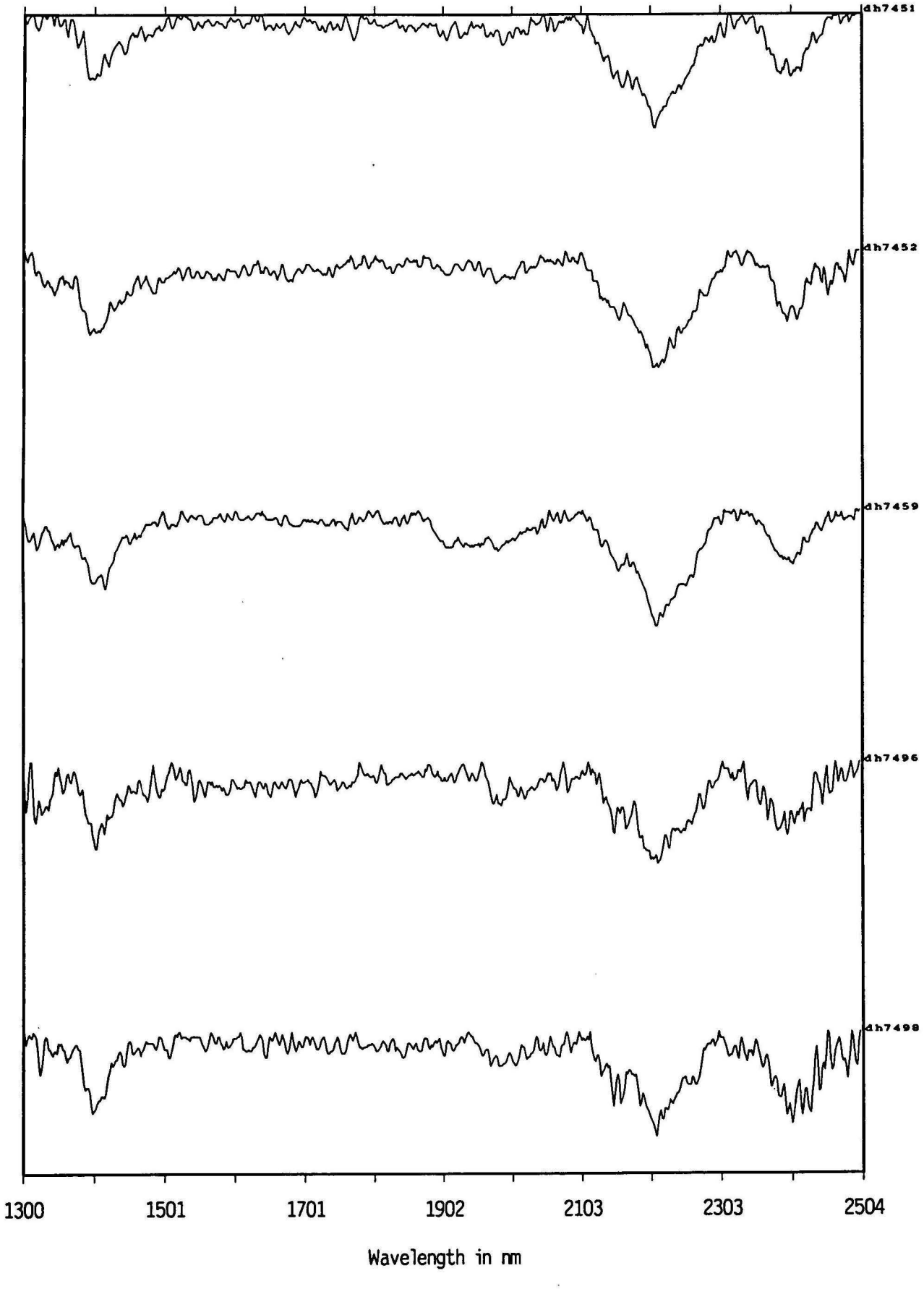

Sulphur Springs group C

PIMAVIEW (C)93 INTEGRATED SPECTRONICS

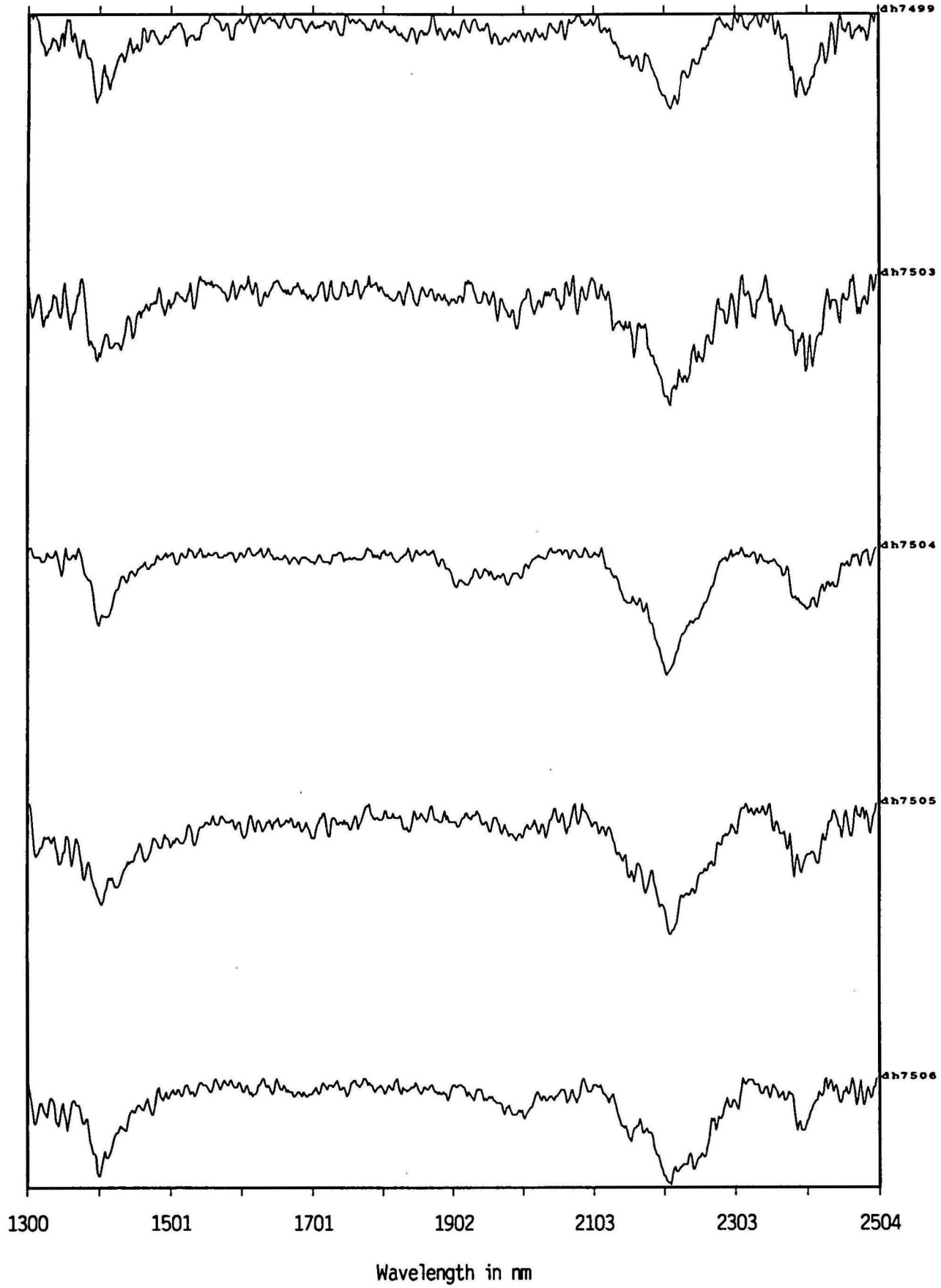

Sulphur Springs group C

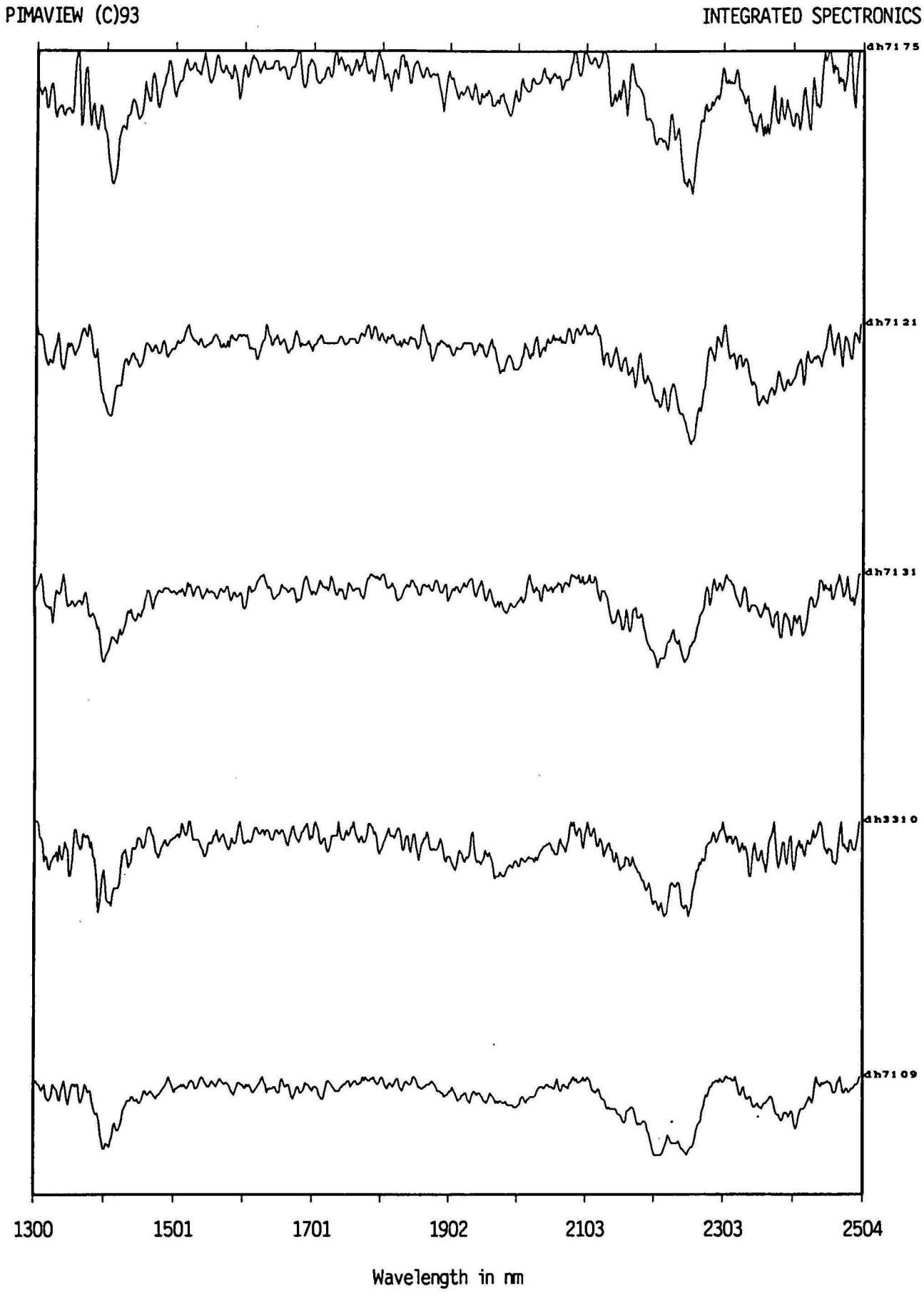

Sulphur Springs group D

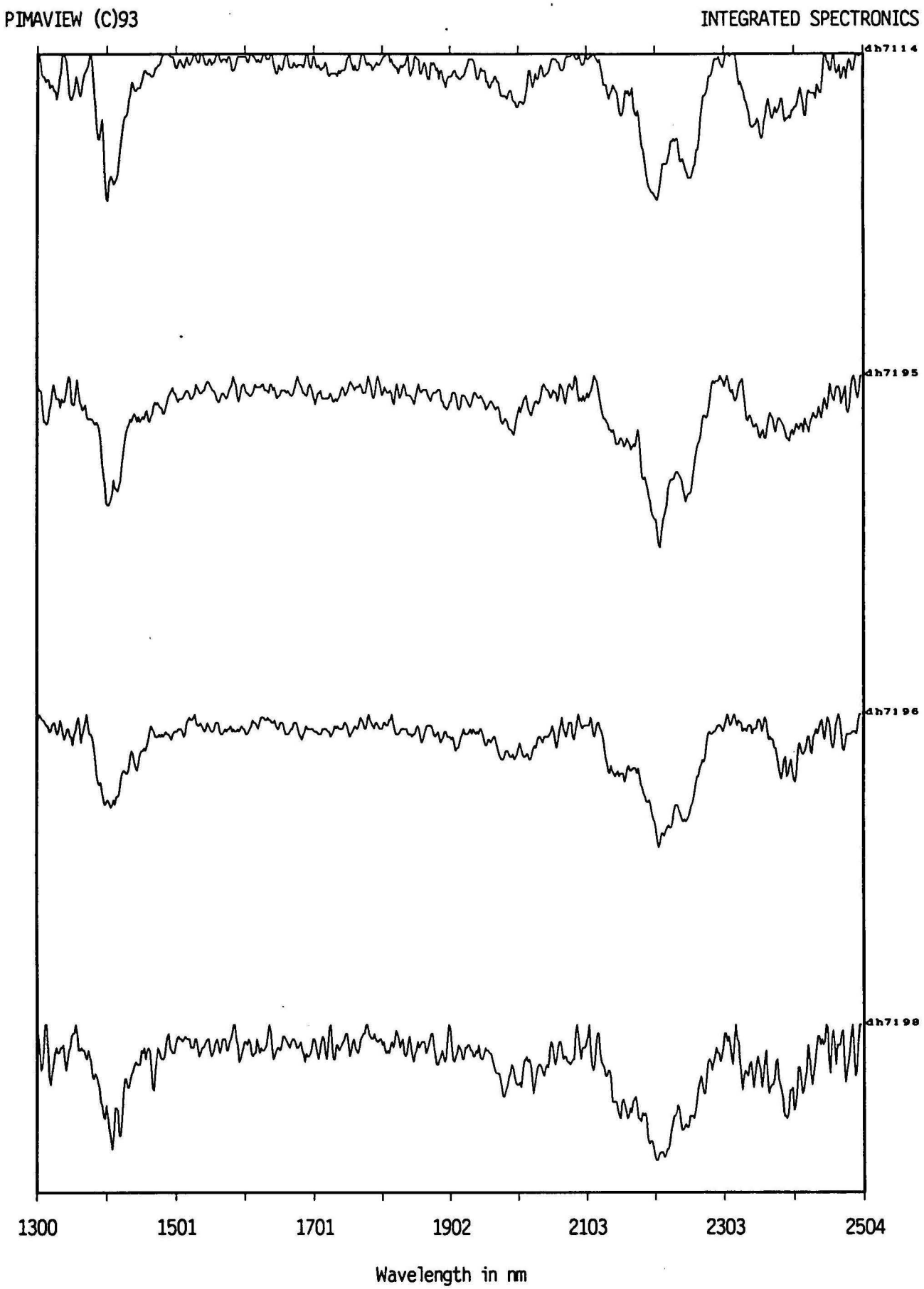

Sulphur Springs group D

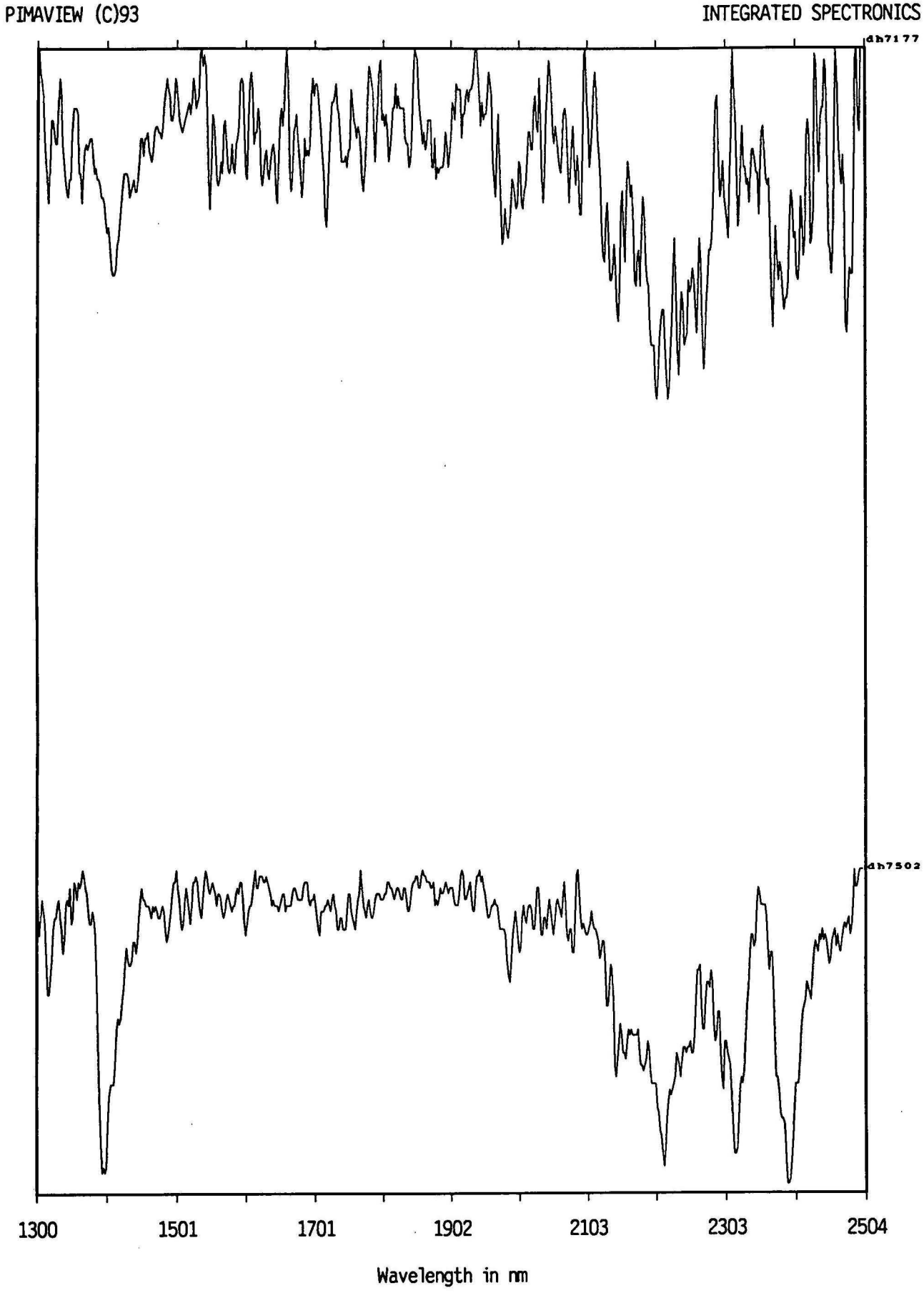

Sulphur Springs other samples